

### Reviewer 3:

Review of 'Atmospheric new particle formation characteristics in the Arctic as measured at Mount Zeppelin, Svalbard, from 2016 to 2018' by Lee et al.

The manuscript studies the characteristics of NPF at Mount Zeppelin, a location in the Arctic far from direct anthropogenic emissions. The study comprises ~2 years of comprehensive valuable data suitable for NPF study. While NPF has been studied at the same location, the new data included in this study contains high time resolution of particle number size distributions of particle sizes relevant for new particle formation. The manuscript is well written, the methods used are clearly described and the literature review is thorough. I suggest publication in ACP after addressing the comments below.

General comments:

1. The exact dates of the measurements need to be reported to identify the reoccurrence of the NPF seasons. The authors mention '89% during the 27 months sampling period', but the exact months need to be mentioned.

Answer: As suggested by the reviewer, we added the detailed sampling period in the manuscript.

Page 6, line 163-164:

"The data coverage for the size distribution data collected by nano-SMPS was about 89% during the 27 months sampling period (Oct 2016 to Dec 2018)."

2. I agree with Anonymous Referee #1 on the necessity of showing the correlation between concentrations of precursor vapours and particle formation rates and growth rates. How do the concentrations of these vary between event days and nonevent days. Something like your figure 9 would be nice to show also for gas-phase precursors. It could be divided into monthly event days and non-event days.

Answer: The reviewer made a good point here. We appreciate for useful comments raised by this reviewer. More analysis on correlations among particle number and gas ( $\text{NH}_3$ ,  $\text{SO}_2$ , and  $\text{H}_2\text{SO}_4$ ) concentrations was conducted. We added the results for daily correlations between 1)  $\text{N}_{3-25}$  and  $\text{SO}_2$ , 2)  $\text{N}_{3-25}$  and  $\text{H}_2\text{SO}_4$  derived from  $\text{SO}_2$ , temperature, RH, CS and solar radiation data, and 3)  $\text{N}_{3-25}$  and  $\text{NH}_3$  concentrations. It was found that the  $\text{SO}_2$  and  $\text{NH}_3$  were not significantly correlated with the  $\text{N}_{3-25}$  (an increasing trend of  $\text{NH}_3$  with the  $\text{N}_{3-25}$  was observed but was not statistically significant). However, the  $\text{N}_{3-25}$  was significantly correlated with the  $\text{H}_2\text{SO}_4$  ( $r = 0.36$ ), suggesting that the  $\text{H}_2\text{SO}_4$  should play an important role in nucleation and growth. The results and discussion on this issue were added in manuscript as follows:

Page 11, line 329-336:

“The  $\text{NH}_3$  concentration was higher on NPF event days than on non-event days as shown in Figure 9 ( $p$ -value  $< 0.001$ ), similar to results shown in Dall’Osto et al. (2017), although daily  $\text{NH}_3$  concentration was not significantly correlated with the  $\text{N}_{3-25}$  as shown in Figure S5 in the Supplement. The  $\text{NH}_3$  in the Arctic can originate from biological and animal sources (e.g., seabird colonies) (Tovar-Sánchez et al., 2010; Croft et al., 2016; Dall’Osto et al., 2017). The  $\text{SO}_2$  was not significantly higher on NPF event days than on non-event days (Figure 9), and not significantly correlated with the  $\text{N}_{3-25}$  (Figure S5 in the Supplement). On the other hand, the  $\text{H}_2\text{SO}_4$  was found to be higher on the NPF event days (Figure 9) and was correlated with the  $\text{N}_{3-25}$  (Figure S5 in the Supplement), suggesting that the  $\text{H}_2\text{SO}_4$  should play an important role in nucleation and growth.”

Revised Figure 9:

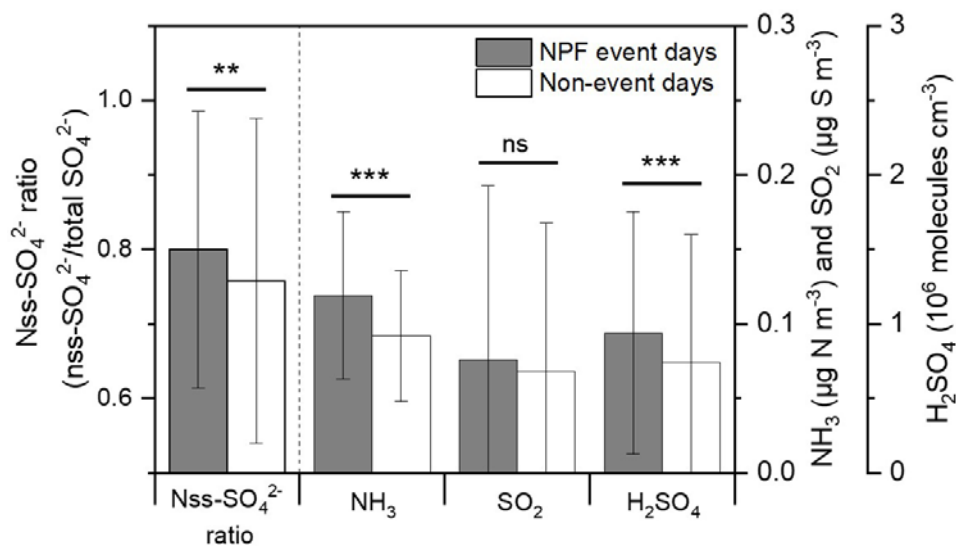
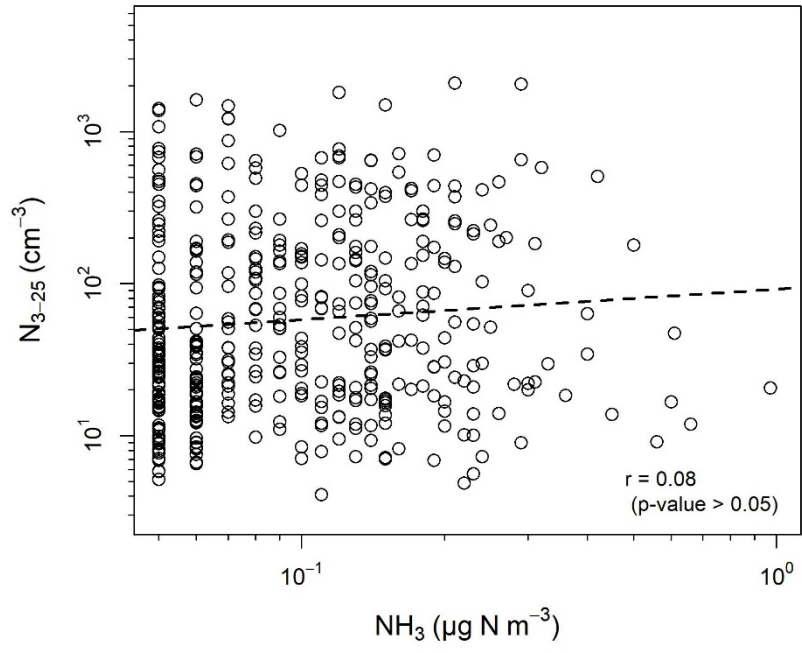
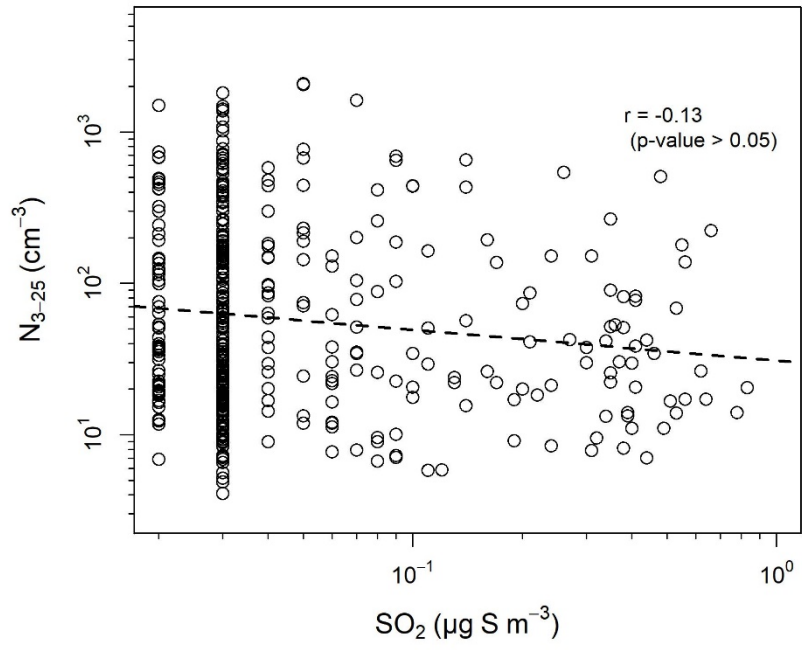


Figure 9. Comparison of average  $\text{nss-SO}_4^{2-}$  ratio ( $\text{nss-SO}_4^{2-}/\text{total SO}_4^{2-}$ ),  $\text{NH}_3$ ,  $\text{SO}_2$ , and  $\text{H}_2\text{SO}_4$  concentrations between NPF events and non-event days: error bar and stars represent the standard deviation and  $p$ -values of a t-test (ns:  $> 0.05$ , \*:  $\leq 0.05$ , \*\*:  $\leq 0.01$ , \*\*\*:  $\leq 0.001$ ), respectively.

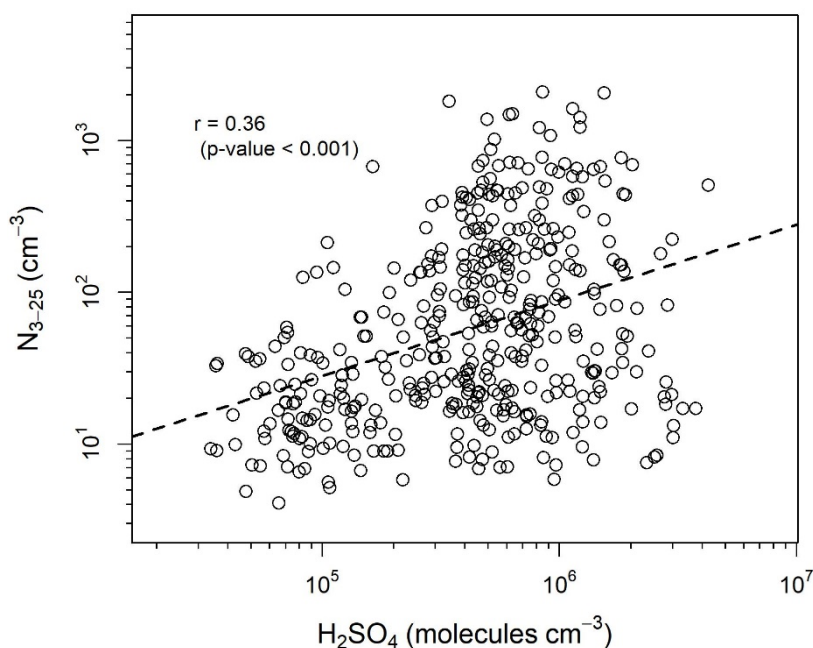
New Figure S5 in the Supplement:



(a)



(b)



(c)

Figure S5. Correlations of daily  $\text{N}_{3-25}$  versus (a) daily  $\text{NH}_3$ , (b) daily  $\text{SO}_2$ , and (c) daily  $\text{H}_2\text{SO}_4$  concentrations during the measurement period. The dashed line represents a linear regression line with a correlation coefficient ( $r$ ).

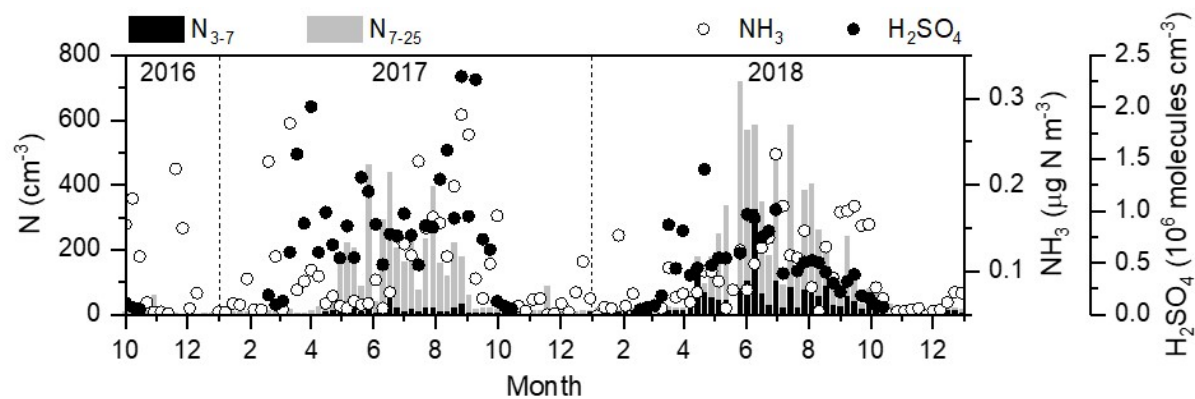
3. The trends of the precursor vapors during the measurement period (sulfuric acid and ammonia), the number concentrations in different clusters, and different modes (3-7 nm, 7-25 nm) as well as the particle formation and growth rates can be shown as daily or weekly medians, maybe in the supplementary. Similar to Kalivitis et al. (2019) figures 8c and 8d or Mikkonen et al. (2020) figure 2.

Answer: We added such information in Figure S4 in the Supplement.

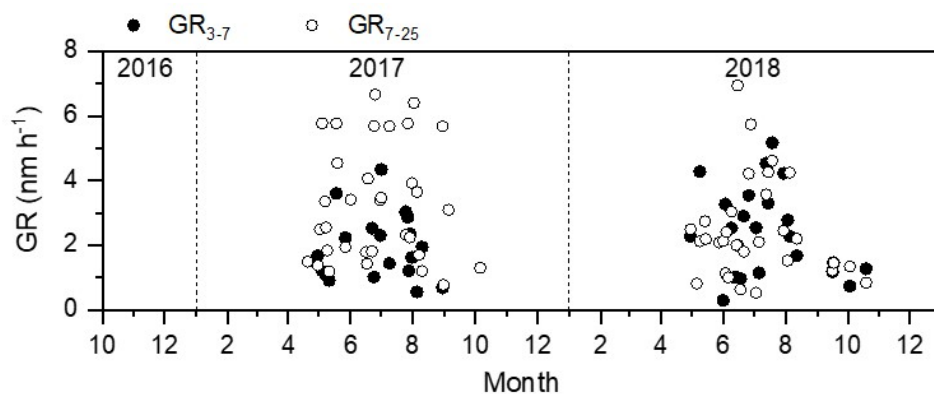
Page 9, line 268-270:

“Time series of daily GR and J in different modes ( $\text{GR}_{3-7}$  and  $\text{J}_{3-7}$ , and  $\text{GR}_{7-25}$  and  $\text{J}_{7-25}$ ), weekly  $\text{N}_{3-7}$  and  $\text{N}_{7-25}$ , and weekly  $\text{NH}_3$  and  $\text{H}_2\text{SO}_4$  are shown in Figure S4 in the Supplement.”

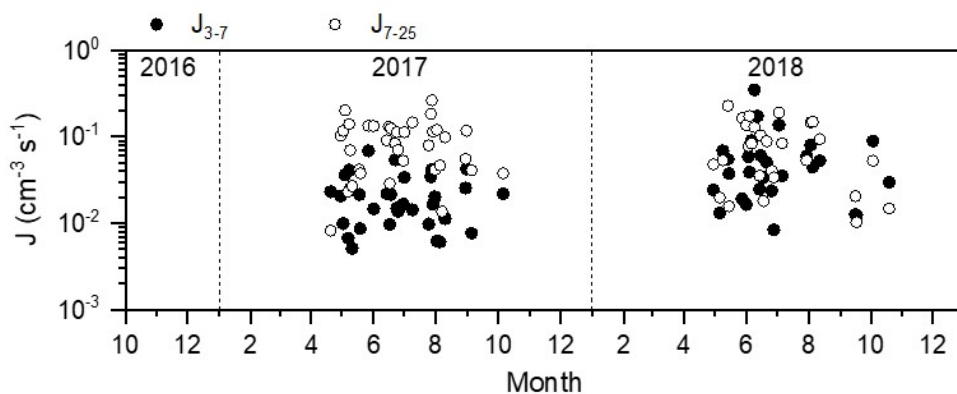
New Figure S4 in the Supplement:



(a)



(b)



(c)

Figure S4. Time series of (a) weekly  $N_{3-7}$ ,  $N_{7-25}$ ,  $NH_3$ , and  $H_2SO_4$ , (b) daily GR and (c) daily J in different modes ( $J_{3-7}$ ,  $J_{7-25}$ ,  $GR_{3-7}$ , and  $GR_{7-25}$ ).

4. You calculate  $J_{3-7}$  but  $GR_{3-25}$ , although the GR is not constant over the size bin 3-25 nm (Kulmala et al., 2013). Calculating a size segregated GR, i.e.  $GR_{3-7}$  and  $GR_{7-25}$  is recommended especially looking at your figure 4 (upper left), the GR is not constant over these sizes.

Answer: The reviewer made a good point. As suggested by the reviewer, GR<sub>3-7</sub> and GR<sub>7-25</sub>, and J<sub>3-7</sub> and J<sub>7-25</sub> were re-calculated, and related Figures were revised.

Page 8-9, line 250-270:

“To determine the characteristics of particle growth, we calculated the GR in the 3–7 nm, 7–25 nm, and 3–25 nm size ranges (i.e., GR<sub>3-7</sub>, GR<sub>7-25</sub>, and GR<sub>3-25</sub>) for NPF events (Figure 7). The average GR<sub>3-25</sub> for all months was 2.66 nm h<sup>-1</sup>, comparable to previously reported GR data (0.2–4.1 nm h<sup>-1</sup>) in the Arctic region (Kerminen et al., 2018). The highest monthly average GR<sub>3-25</sub> was observed in July (3.03 nm h<sup>-1</sup>) and the maximum individual value (6.54 nm h<sup>-1</sup>) occurred in June. The averages of GR<sub>3-7</sub> and GR<sub>7-25</sub> were 2.07 nm h<sup>-1</sup> and 2.85 nm h<sup>-1</sup>, respectively. However, the GR was much lower than the values observed in typical urban areas (Table 1), suggesting a lower availability of condensing vapors contributing to particle growth in the Arctic atmosphere. The formation rates of particles in the same size range as calculated GR were also derived. The averages of J<sub>3-7</sub>, J<sub>7-25</sub>, and J<sub>3-25</sub> during NPF events were 0.04 cm<sup>-3</sup> s<sup>-1</sup>, 0.09 cm<sup>-3</sup> s<sup>-1</sup> and 0.12 cm<sup>-3</sup> s<sup>-1</sup>, respectively. The highest monthly average and maximum for J<sub>3-7</sub> were both found in June, but for J<sub>7-25</sub> and J<sub>3-25</sub> were found in July. The formation rates (relative standard deviation (RSD) = 39–44%) varied by month more significantly than for GR (RSD = 27–33%). The formation rates in this study were much lower than those reported in continental areas (Stanier et al., 2004; Hamed et al., 2007; Wu et al., 2007; Manninen et al., 2010; Xiao et al., 2015; Shen et al., 2016; Cai et al., 2017). A good linear relationship was found between J<sub>3-7</sub> and N<sub>3-7</sub> ( $r = 0.97$  and  $p$ -value < 0.001) as shown in Figure S3 in the Supplement, indicating that 3–7 nm particles were produced by gas-to-particle conversion rather than direct emissions in the particle phase (i.e., not primary) (Kalivitis et al., 2019). No significant correlation was found between J<sub>3-7</sub> and GR<sub>3-7</sub>, suggesting that the vapors participating in the early stage of NPF could be at least partly different from the vapors contributing to subsequent particle growth (Nieminen et al., 2014). However, detailed chemical data for nanoparticles during formation and growth should be obtained to achieve complete understanding of the participating chemical species. Our data indicate that, although NPF occurrence frequency in the Arctic was comparable to continental areas, the J and GR were much lower. Time series of daily GR and J in different modes (GR<sub>3-7</sub> and J<sub>3-7</sub>, and GR<sub>7-25</sub> and J<sub>7-25</sub>), weekly N<sub>3-7</sub> and N<sub>7-25</sub>, and weekly NH<sub>3</sub> and H<sub>2</sub>SO<sub>4</sub> are shown in Figure S4 in the Supplement.”

New Figure S3 in the Supplement:

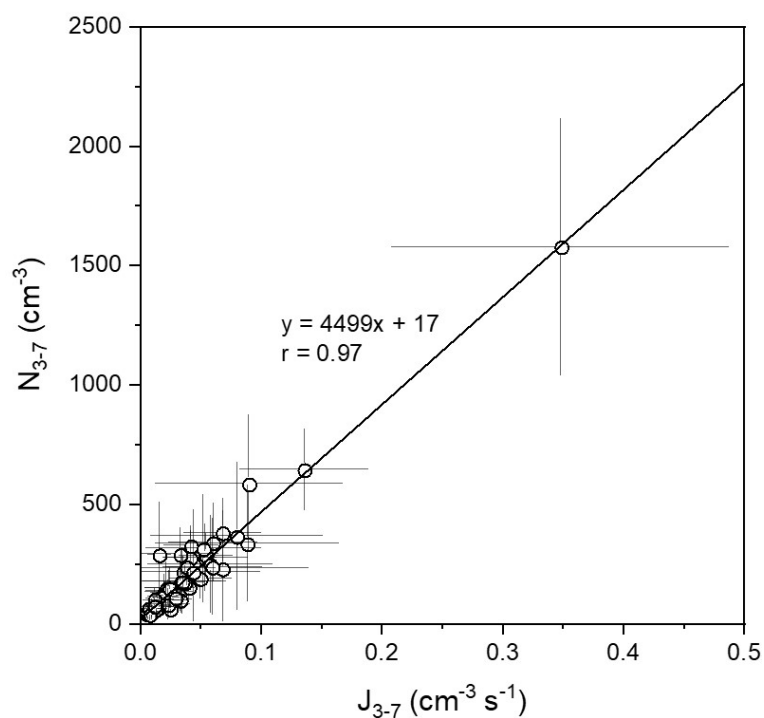


Figure S3. Relationship between  $N_{3-7}$  and  $J_{3-7}$  during NPF events with a linear regression line and a correction coefficient ( $r$ ).

5. I don't understand why you chose to present the data in UTC and not Local time. When using UTC, there is no relevance to solar radiation or to other locations. Please show your figures in local time (Figure 4 and Figure 5-middle). You can also show figure 5-middle relative to sunrise. See for example figure 6 in Dada et al. (2018).

Answer: As suggested by the reviewer, the UTC time was changed into the local time as shown in Figures 4 and 5.

6. What about nighttime clustering? your figure middle panel shows that the start time of NPF is around 20 UTC? also unit of time needs to be added to the figure or caption.

Answer: The unit of time was added in the figure and caption. The nighttime NPF also occurred in late fall to winter (20% out of total NPF events). The exact mechanism for this NPF was unclear to us. Nanoparticles formed at earlier times (daytime) in other places may be transported to the site during nighttime (Vehkamäki et al., 2004; Park et al., 2020). The discussion was added in manuscript as follows:

Page 8, Line 237-239:

“The nighttime NPF also occurred in late fall to winter (20% out of total NPF events). The exact mechanism for this NPF was unclear. Nanoparticles formed at earlier times (daytime) in other places may be transported to the site during nighttime (Vehkamäki et al., 2004; Park et al., 2020).”

7-1. There seems to be an effect of temperature as well as CS on the probability of NPF. See figure 13 in Dada et al. (2017).

Answer: As suggested by the reviewer, we discussed the effect of temperature on the NPF probability. A similar figure to the Dada et al. (2017) was also added in the Supplement (Figure S6).

Page 11, line 338-341:

“The NPF event probability distribution with daily CS and temperature was included in Figure S6 in the Supplement. The NPF event probability was calculated by the ratio of the NPF event days per total days for the given CS and temperature. The NPF event probability increased at moderate temperatures when the CS was low, while when the CS was high, the probability increased at relatively high temperature as shown in Figure S6 in the Supplement.”

New Figure S6 in the Supplement:

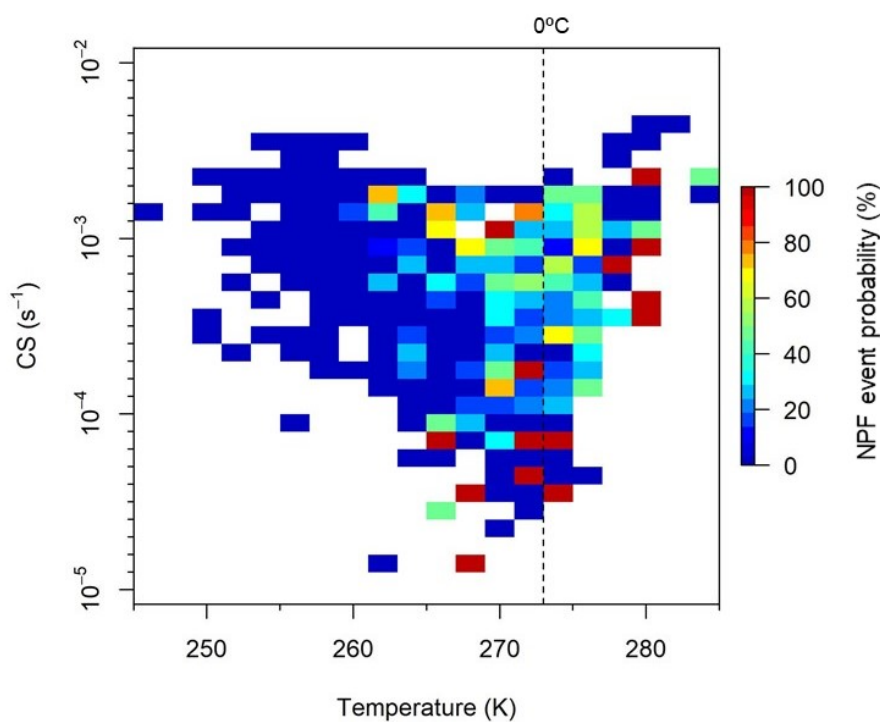


Figure S6. NPF event probability distribution with daily CS and temperature. The cell size was 2 K (temperature) by the ratio of 1.26 between two consecutive CS values.

7-2. Does the occurrence of Arctic haze inhibit 3 nm clustering and growth?

Answer: The NPF still occurred during the Arctic haze period (April-May), but the NPF occurrence frequency was lower than summer. Refer to our previous statements as given below.

Page 7, line 216-223:



“Our results showed that NPF occurrence increased significantly in April, was maintained at a high level from May to August, then decreased in September and October. The average values of CS during NPF event and non-event days were  $0.57 \times 10^{-3} \text{ s}^{-1}$  and  $0.69 \times 10^{-3} \text{ s}^{-1}$ , respectively. The higher biological and photochemical activity, lower transport of pollutants from mid-latitudes, and increased wet scavenging of particles (low CS) in summer likely favored NPF (Ström et al., 2009). In addition, the melting of sea ice in summer can increase the availability of marine biogenic sources, promoting NPF (Quinn et al., 2008; Tovar-Sánchez et al., 2010; Dall’Osto et al., 2018). Overall, NPF occurrence is mainly affected by the availability of solar radiation (photochemistry) and gaseous precursors in addition to the survival probability of clusters or particles (Kulmala et al., 2017).”

7-3. How different is the CS between NPF event days and non-event days? If possible, you could examine how CS varies between the air mass clusters.

Answer: As suggested by the reviewer, we compared CS during NPF event and non-event days. Also, information on air mass-dependent CS was added.

Page 7, line 218-219:

“The average values of CS during NPF event and non-event days were  $0.57 \times 10^{-3} \text{ s}^{-1}$  and  $0.69 \times 10^{-3} \text{ s}^{-1}$ , respectively.”

Page 9, line 282-284:

“The CS values were  $0.54 \times 10^{-3} \text{ s}^{-1}$ ,  $0.74 \times 10^{-3} \text{ s}^{-1}$ ,  $0.77 \times 10^{-3} \text{ s}^{-1}$ ,  $0.64 \times 10^{-3} \text{ s}^{-1}$ , and  $0.80 \times 10^{-3} \text{ s}^{-1}$  for cluster 1, cluster 2, cluster 3, cluster 4, and cluster 5, respectively, indicating that the cluster 1 had the lowest CS.”

8. Why GR3-25 while N3-20? Maybe use 3- 25 nm as nucleation mode for consistency with your GR calculations and with previous literature. N3-25 has been referred to as nucleation mode particles in some literature (Vana et al., 2016; Zhou et al., 2020).

Answer: As suggested by the reviewer,  $N_{3-25}$ , and  $N_{25-60}$  were used in texts and related Figures (Figure 2, 4, and 8).

9. Comparison of instruments: how does your nano-smps compare to the instruments at the station? See figure 1 in Kangasluoma et al. (2020).

Answer: We compared our nano-SMPS data with DMPS data at the same station as shown in Figure S1 in the Supplement, suggesting that they were in a good agreement.

Page 6, line 165-167:

“We compared our nano-SMPS data with DMPS data at the same station as shown in Figure S1 in the Supplement, suggesting that they were in a good agreement.”

New Figure S1 in the Supplement:

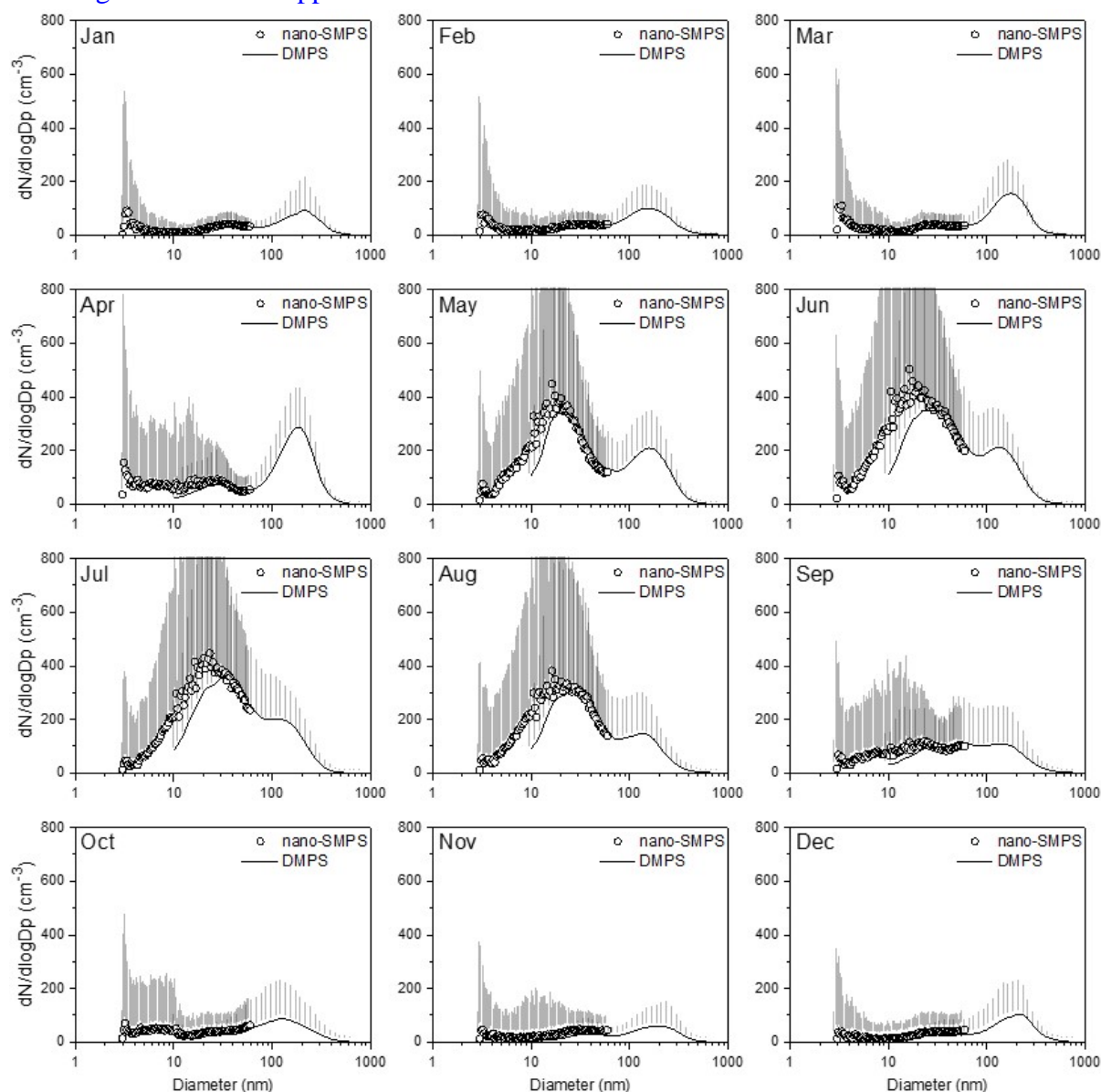


Figure S1. Comparison of monthly average size distributions obtained from the nano-SMPS (3–60 nm) and DMPS (10–810 nm). The error bars indicate standard deviation.

Specific comments:

Line 14: “ a higher resolution than ever before”, this sentence needs to be changed since previous studies have shown up to 10 s time resolution, unless you mean at the specific location you are measuring. Please change here and elsewhere.

Answer: We originally intended “size” resolution, so we added “size” as follows:  
“...a higher size resolution than ever before”

Line 36, anytime, do you mean anytime during the month? or anytime during the day? because very little nighttime NPF that grows to full NPF events are observed in the boundary layer.

Answer: The “anytime” was modified to “anywhere”.

Line 38, survivor —> survival

Answer: The “survivor” was changed to “survival”.

Line 175, ‘Dall Maso’ -> Dal Maso.

Answer: We corrected the name.

Line 190, survivable -> survival

Answer: The “survivable” was changed to “survival”.

# 1 Atmospheric new particle formation characteristics in the Arctic as 2 measured at Mount Zeppelin, Svalbard, from 2016 to 2018

3 Haebum Lee<sup>1</sup>, KwangYul Lee<sup>1</sup>, Chris Rene Lunder<sup>2</sup>, Radovan Krejci<sup>3</sup>, Wenche Aas<sup>2</sup>, Jiyeon Park<sup>4</sup>, Ki-  
4 Tae Park<sup>4</sup>, Bang Yong Lee<sup>4</sup>, Young-Jun Yoon<sup>4,\*</sup>, and Kihong Park<sup>1,\*</sup>

5 <sup>1</sup>School of Earth Sciences and Environmental Engineering, Gwangju Institute of Science and Technology, 123  
6 Cheomdangwagi-ro, Buk-gu, Gwangju 61005, Republic of Korea.

7 <sup>2</sup>Department for Atmospheric and Climate Research, NILU - Norwegian Institute for Air Research, Kjeller, Norway.

8 <sup>3</sup>Department of Environmental Sciences and the Bolin Centre for Climate Research, Stockholm University, Stockholm, SE-  
9 106 91, Sweden.

10 <sup>4</sup>Korea Polar Research Institute, 26, Songdo Mirae-ro, Yeonsu-Gu, Incheon, Korea.

11

12 \*Correspondence to: Kihong Park (kpark@gist.ac.kr) and Young-Jun Yoon (yjyoon@kopri.re.kr)

13 **Abstract.** We conducted continuous measurement of nanoparticles down to 3 nm size in the Arctic at Mount Zeppelin, Ny  
14 Ålesund, Svalbard, from 2016 to 2018, providing a size distribution of nanoparticles (3–60 nm) **with a higher size resolution**  
15 **than ever before**. A significant number of nanoparticles as small as 3 nm were often observed during new particle formation  
16 (NPF), particularly in summer, suggesting that these were likely produced near the site rather than being transported from  
17 other regions after growth. The average NPF frequency per year was 23% having the highest percentage in August (63%). **The**  
18 **average formation rate (J) and growth rate (GR) for 3–7 nm particles were 0.04 cm<sup>-3</sup> s<sup>-1</sup> and 2.07 nm h<sup>-1</sup>, respectively**. Although  
19 NPF frequency in the Arctic was comparable to that in continental areas, the J and GR were much lower. The number of  
20 nanoparticles increased more frequently when air mass originated over the south and southwest ocean regions; this pattern  
21 overlapped with regions having strong chlorophyll- $\alpha$  concentration and dimethyl sulfide (DMS) production capacity  
22 (southwest ocean), and was **also associated with increased NH<sub>3</sub> and H<sub>2</sub>SO<sub>4</sub> concentration**, suggesting that marine biogenic  
23 sources were responsible for gaseous precursors to NPF. Our results show that previously developed NPF occurrence criteria  
24 (low loss rate and high cluster growth rate favor NPF) are also applicable to NPF in the Arctic.

## 25 1 Introduction

26 The Arctic climate system is affected by the region's snow-covered land, sea ice, and ocean, making the region  
27 vulnerable to global climate change (Jeffries and Richter-Menge, 2012). Greenhouse gases and aerosols are significant factors  
28 affecting the regional climate (Quinn et al., 2007; IPCC, 2014). In particular, aerosols in the ambient atmosphere affect the  
29 radiation balance by scattering or absorbing incoming solar light (direct effect) (Toon and Pollack, 1980; Satheesh et al., 2005)  
30 and forming clouds by acting as cloud condensation nuclei (CCN) (indirect effect) (Merikanto et al., 2009).

31 New particle formation (NPF), which significantly enhances the number of particles in the ambient atmosphere, has  
32 been observed in various locations and at various times (Kulmala et al., 2004; Wang et al., 2017; Yu et al., 2017). In favourable  
33 conditions, newly formed nanoparticles can, through condensation and coagulation, grow to sizes allowing the formation of  
34 CCN. NPF is observed regardless of pollution level, from very clean (e.g., background sites) to heavily polluted (e.g., urban  
35 sites), suggesting that various pathways are involved depending on the location and time (Kulmala et al., 2004; Wang et al.,  
36 2017). Nucleation can occur almost [anywhere](#) in diverse environments, but NPF is observed only when freshly nucleated  
37 clusters grow to a detectable size (1–3 nm) (McMurry et al., 2010). Previously developed criteria for NPF occurrence suggest  
38 that a low loss (or scavenging) rate and high growth rate (GR) of clusters increase fresh nuclei [survival](#) probability and thus  
39 favoring NPF, while a high loss rate and low cluster GR suppress it (Kuang et al., 2012).

40 In the Arctic, specific phenomenon called “Arctic haze” related to long range transport of polluted air masses  
41 typically occurs in the late winter and early spring (Iziomon et al., 2006; O’Neill et al., 2008, Hirdman et al., 2010). The Arctic  
42 haze is associated with elevated concentrations of accumulation-mode particles. (Radke et al., 1984; Shaw, 1995; Law and  
43 Stohl, 2007; Quinn et al., 2007). High concentration of accumulation-mode particles results in a high condensational sink (CS)  
44 for precursor vapors, which could suppress NPF. The NPF in the Arctic was often reported in summer, when the CS was  
45 smaller (Wiedensohler et al., 1996; Covert et al., 1996; Sharma et al., 2013; Willis et al., 2016; Croft et al., 2016). In addition,  
46 strong biogenic production from marine and coastal environments in the Arctic region (e.g., Alaska, Alert, and Svalbard) was  
47 reported to be linked to NPF due to an increased amount of biogenic sulfur compounds such as dimethyl sulfide and its  
48 oxidative products (methane sulfonate and biogenic sulfate) (Leaitch et al., 2013; Park et al., 2017). Like in sulfuric acid-rich  
49 regions, organic-based new particles were observed in pristine environments (Quinn et al., 2002; [Karl et al., 2013](#); Leaitch et  
50 al., 2013; Heintzenberg et al., 2015). Asmi et al. (2016) reported that NPF was more common in air masses of oceanic origin  
51 compared to continental ones in the Arctic (Tiksi station, Russia). Dall’Osto et al. (2018) suggested that NPF at Station Nord  
52 in North Greenland was related to seasonal sea-ice cycles (i.e., the NPF was associated with air masses coming from open  
53 water and melting sea-ice regions).

54 There are several past studies of NPF at the Zeppelin Observatory at Mount Zeppelin in Svalbard, Norway (Tunved  
55 et al., 2013; Dall’Osto et al., 2017; Heintzenberg et al., 2017). The location of the station is 474 m above sea level and ~2 km  
56 from a small scientific community, with minimal effects from anthropogenic sources; its unique geographical location is ideal  
57 for investigating NPF in the Arctic environment. Tunved et al. (2013) studied seasonal variations in particle size distribution  
58 and NPF based on aerosol size distribution data (10–790 nm) from 2000 to 2010. Heintzenberg et al. (2017) developed a new  
59 NPF search algorithm using size distribution data (5–630 nm) from 2006 to 2015. Dall’Osto et al. (2017) determined the  
60 relationship between NPF and the extent of Arctic sea-ice melt using size distribution data (10–500 nm) from 2000 to 2010  
61 and used hourly data to classify the size distributions and NPF types. It was reported that NPF at the Mount Zeppelin site  
62 mostly occur during summer, which was attributed to the low CS and high biological activity in summer (Leaitch et al., 2013;  
63 Heintzenberg et al., 2015; Park et al., 2017). NPF occurrence was low during the Arctic haze (with high CS) period (Tunved  
64 et al., 2013; Croft et al., 2016). Heintzenberg et al. (2017) suggested that NPF at the Mount Zeppelin site was related to solar

65 flux and sea surface temperature, affecting marine biological processes and photochemical reactions with less CS. They  
66 reported the potential source regions for NPF to be the marginal-ice and open-water areas between northeastern Greenland and  
67 eastern Svalbard. Although particle size distribution data from the Mount Zeppelin site are available (Ström et al., 2003;  
68 Tunved et al., 2013; Dall'Osto et al., 2017; Heintzenberg et al., 2017), no data regarding the size distribution of nanoparticles  
69 smaller than 5 nm are available, though these could provide greater insight into NPF characteristics. Currently, the initial  
70 formation and growth of nanoparticles below 10 nm cannot be resolved, and weak NPF events with no substantial particle  
71 growth up to 10 nm cannot be detected.

72 In this study, we measured **number** size distribution of nanoparticles down to 3 nm for the first time at Zeppelin  
73 station, and obtained continuous size distributions of 3–60 nm particles every 3 min from 2016 to 2018. This allowed the size  
74 distribution of nanoparticles to be determined **with a higher size resolution than ever before**, enabling better identification of  
75 whether freshly nucleated particles formed on-site or were transported from other regions after substantial growth. We were  
76 also able to detect NPF events when particle growth was terminated below 10 nm. The particle size distributions were classified  
77 into several clusters, and the seasonal (monthly), daily, and diurnal variations of the nanoparticle concentrations were examined.  
78 We also applied the NPF criteria to Arctic data to determine whether or not NPF should occur and investigated the  
79 characteristics of NPF events related to formation rate, GR, CS, and meteorological parameters. Finally, potential source  
80 regions for NPF were explored using air mass backward trajectory and satellite-derived chlorophyll- $\alpha$  concentration data. **The**  
81 **chlorophyll- $\alpha$  which is involved in oxygenic photosynthesis in ocean has been considered as a proxy for phytoplankton biomass**  
82 **only. Recent studies showed that there was a strong correlation between sea-surface chlorophyll- $\alpha$  concentration (estimated**  
83 **by MODIS-aqua) and atmospheric DMS levels at Zeppelin station (Park et al., 2013; Park et al., 2018).**

## 84 **2 Methods**

85 The measurement site was located at the Zeppelin Observatory at Mount Zeppelin, Svalbard (78°54'N, 11°53'E),  
86 which is 474 m above sea level and ~2 km from the small scientific community in Ny-Ålesund, Norway (78°55'N, 11°56'E)  
87 (Figure 1). Ny-Ålesund lies within the west Spitsbergen current at the northernmost point of the warm Atlantic influx; this  
88 location provides an ideal location for observing climate parameters and investigating the long-range transport route by which  
89 contamination is often carried via southerly air masses (Neuber et al., 2011). The dominant wind patterns (east and southeast  
90 from the Kongsvegen glacier (40%) and northwest from the Kongsfjorden channels (14%) during the measurement period)  
91 and elevation suggest that the effects of local sources on the Zeppelin Observatory are small (Beine et al., 2001).

92 An air inlet with a flow rate of 100 L min<sup>-1</sup> was used to introduce ambient aerosols into the instruments. The flow  
93 temperature was maintained above 0°C to prevent ice and frost formation in the tube. The observatory was kept warm and dry,  
94 with an indoor temperature and relative humidity (RH) of ~20°C and < 30%, respectively (Tunved et al., 2013; Heintzenberg  
95 et al., 2017). A nano-scanning mobility particle sizer consisting of a nano-differential mobility analyzer (nano-DMA) (model  
96 3085, TSI, USA) and an ultrafine condensation particle counter (model 3776, TSI, USA) was used to measure the size

97 distribution of nanoparticles (3–60 nm) every 3 min; the aerosol flow rate was 1.5 L min<sup>-1</sup> and the sheath flow rate was 15 L  
98 min<sup>-1</sup>. The size distribution data were processed using the method described by Kulmala et al. (2012).

99 Daily ionic species (Na<sup>+</sup>, Mg<sup>2+</sup>, K<sup>+</sup>, NH<sub>4</sub><sup>+</sup>, NO<sub>3</sub><sup>-</sup>, SO<sub>4</sub><sup>2-</sup>, and Cl<sup>-</sup>) in particulate matters and gas data (NH<sub>3</sub> and SO<sub>2</sub>)  
100 at Zeppelin Observatory, along with meteorological parameters (temperature, RH, wind, and pressure), were obtained from  
101 the Norwegian national monitoring program (Aas et al., 2019) via the EBAS database (<http://ebas.nilu.no/>). Daily ionic species  
102 and gas data are daily measurements collected with a 3-stage filterpack sampler (NILU prototype) with no pre-impactor. The  
103 size cut off of the inlet section is approximately 10 µm. Field blanks were prepared in the same as the other samples. It should  
104 be noted that for the nitrogen compounds the separation of gas and aerosol might be biased due to the volatile nature of NH<sub>4</sub>NO<sub>3</sub>.  
105 The detection limits were 0.05 µg N m<sup>-3</sup> and 0.01 µg S m<sup>-3</sup> for NH<sub>3</sub> and SO<sub>2</sub>, respectively, and 0.01 µg m<sup>-3</sup> for Na<sup>+</sup>, Mg<sup>2+</sup>, K<sup>+</sup>,  
106 NH<sub>4</sub><sup>+</sup>, and Cl<sup>-</sup>, 0.01 µg N m<sup>-3</sup> for NO<sub>3</sub><sup>-</sup>, and 0.01 µg S m<sup>-3</sup> for SO<sub>4</sub><sup>2-</sup>. The data quality management and system are accredited  
107 in accordance to NS-EN ISO / IEC 1702 standards. The detailed information of sampling method and analysis can be found  
108 elsewhere (EMAP 2014; Aas et al., 2019). Solar radiation (SRAD) at the AWIPEV (the Alfred Wegener Institute Helmholtz  
109 Centre for Polar and Marine Research and the French Polar Institute Paul Emile Victor) observatory in Ny-Ålesund were  
110 obtained from the Baseline Surface Radiation Network (BSRN) (Maturilli, 2019). Hourly data for number size distributions  
111 of particles from 5–810 nm and 10–790 nm, measured with discrete mobility particle sizers (DMPS), were obtained from  
112 Stockholm University and the Norwegian Institute for Air Research (NILU), respectively. The data from the DMPS and  
113 filterpack measurements are reported to several international monitoring programmes (EMEP (European Monitoring and  
114 Evaluation Programme), ACTRIS (Aerosols, Clouds and Trace gases Research InfraStructure Network), and GAW-WDCA  
115 (Global Atmospheric Watch-the World Data Centre for Aerosols)), and they are openly available from the database  
116 infrastructure EBAS. In addition, the hourly black carbon (BC) data at Zeppelin were used to examine the effect of primary  
117 combustion sources on the NPF.

118 Satellite-derived chlorophyll-*a* concentration data in the Svalbard region (70–85°N, 25°W–50°E) was obtained from  
119 the level-3 product of the Aqua-Moderate Resolution Imaging Spectroradiometer (MODIS) at a 4 km resolution. Air mass  
120 backward trajectories arriving at the Zeppelin Observatory were calculated for up to 5 days using the National Oceanic and  
121 Atmospheric Administration (NOAA) Hybrid Single Particle Lagrangian Integrated Trajectory (HYSPLIT) model based on  
122 Global Data Assimilation System (GDAS) 1° data. A potential source contribution function (PSCF) method (Pekney et al.,  
123 2006; Wang et al., 2009; Fleming et al., 2012) was also used to relate the air mass to NPF occurrence by analyzing the residence  
124 time of the air mass relative to the concentration of nanoparticles at the receptor site (Wang et al., 2009). In addition, the k-  
125 means clustering method, an unsupervised data classification/partitioning approach, was used to classify potential air mass  
126 origin along with the size distributions (Beddows et al., 2009; Dall'Osto et al., 2017).

127 The particle GR was calculated as the change rates of representative particle diameters (*d*<sub>1</sub> and *d*<sub>2</sub>) with the highest  
128 concentrations at particular times (*t*<sub>1</sub> and *t*<sub>2</sub>) (Hussein et al., 2005; Kulmala et al., 2012). The CS, which determines how rapidly  
129 condensable vapor molecules will condense on the existing aerosols (Kulmala et al., 2012), was calculated from the size  
130 distribution data (3–810 nm) with an assumed H<sub>2</sub>SO<sub>4</sub> diffusion coefficient of 0.117 cm<sup>2</sup> s<sup>-1</sup> (Gong et al., 2010; Cai et al., 2017).



131 The number concentration in the size range  $d_i$  to  $d_j$  ( $N_{i-j}$ ) was derived from the measured size distribution data. Considering the  
 132 particle loss and production processes allowed the following balance equation for  $N_{i-j}$  to be derived:

$$133 \frac{dN_{i-j}}{dt} = J_{i-j} - F_{\text{coag}} - F_{\text{growth}} \quad (1)$$

134 where  $J_{i-j}$  is the particle formation rate in the size range of  $d_i$  to  $d_j$ ,  $F_{\text{coag}}$  is the particle loss rate related to coagulation scavenging  
 135 in the size range of  $d_i$  to  $d_j$ , and  $F_{\text{growth}}$  is the condensational GR of the nucleation-mode particles. Based on methods suggested  
 136 by Kulmala et al. (2012), the particle formation rate ( $J_{i-j}$ ) was calculated as:

$$137 J_{i-j} = \frac{dN_{i-j}}{dt} + \frac{N_{i-j}}{d_j - d_i} \cdot \text{GR} + N_{i-j} \text{CoagS}_{i-j} \quad (2)$$

138 where  $\text{CoagS}_{i-j}$  represents the mean of the coagulation sink (CoagS) in the size range of  $d_i$  to  $d_j$ .

139 The dimensionless criterion ( $L_\Gamma$ ), which can be used to predict the occurrence of NPF events (McMurry et al., 2005;  
 140 Cai et al., 2017), was calculated as:

$$141 L_\Gamma = \frac{\bar{c}_1 A_{\text{Fuchs}}}{4\beta_{11} N_1 \Gamma} \quad (3)$$

142 where  $\bar{c}_1$  is the mean thermal velocity of vapor ( $\text{H}_2\text{SO}_4$ ),  $A_{\text{Fuchs}}$  is the Fuchs surface area (a coagulation scavenging parameter),  
 143  $\beta_{11}$  is the free molecule collision frequency function for monomer collisions,  $N_1$  is the  $\text{H}_2\text{SO}_4$  molecular concentration during  
 144 the nucleation event, and  $\Gamma$  is the growth enhancement factor obtained by dividing the measured GR by the growth determined  
 145 based on the condensation of only  $\text{H}_2\text{SO}_4$ . The  $\text{H}_2\text{SO}_4$  molecular concentration was predicted from the measured daily  $\text{SO}_2$ ,  
 146 hourly CS, hourly solar radiation, and hourly meteorological data (RH and temperature) using the method proposed by  
 147 Mikkonen et al. (2011). The empirical proxy model of  $\text{H}_2\text{SO}_4$  is given by:

$$148 [\text{H}_2\text{SO}_4] = a \cdot k \cdot [\text{SO}_2]^b \cdot \text{SRAD}^c \cdot (\text{CS} \cdot \text{RH})^d \quad (4)$$

149 where  $[\text{SO}_2]$  is the  $\text{SO}_2$  molecular concentration ( $\text{molecules cm}^{-3}$ ), SRAD is the solar radiation ( $\text{W m}^{-2}$ ), CS is the condensation  
 150 sink ( $\text{s}^{-1}$ ), RH is the relative humidity (%), and  $k$  is the reaction rate constant depending on ambient temperature (see detailed  
 151 definition for  $k$  in Eq. (3) of Mikkonen et al., 2011) with coefficients of  $a = 8.21 \times 10^{-3}$ ,  $b = 0.62$ ,  $c = 1$ , and  $d = -0.13$ . The  
 152  $\text{H}_2\text{SO}_4$  concentration at Zeppelin was  $5.98 \times 10^4$ – $3.19 \times 10^6$   $\text{molecules cm}^{-3}$  during the summer in 2008 (Giamarelou et al., 2016)  
 153 which is in a similar range to ours ( $2.69 \times 10^4$ – $7.68 \times 10^6$   $\text{molecules cm}^{-3}$ ) in 2016–2018.



### 162 3 Results and discussion

163 The data coverage for the size distribution data collected by nano-SMPS was about 89% during the 27 months  
164 sampling period (Oct 2016 to Dec 2018). The monthly variations of the number concentrations of the 3–20 nm nanoparticles  
165 ( $N_{3-25}$ ) and 25–60 nm nanoparticles ( $N_{25-60}$ ) in 2016–2018 (averaged from hourly data) are shown in Figure 2. We compared  
166 our nano-SMPS data with DMPS data at the same station as shown in Figure S1 in the Supplement, suggesting that they were  
167 in a good agreement. Both  $N_{3-25}$  and  $N_{25-60}$  were highest in summer and lowest in winter, indicating that NPF occurred  
168 frequently in summer. The higher SRAD and lower CS (calculated from the 3–810 nm size distribution data) in summer also  
169 favored nanoparticle production. The highest monthly SRAD ( $199 \text{ W m}^{-2}$ ) was observed in June. Due to the higher latitude of  
170 the site, the SRAD was lower than values reported at other continental sites ( $449 \text{ W m}^{-2}$  during NPF in Lanzhou, China (Gao  
171 et al, 2011);  $442\text{--}445 \text{ W m}^{-2}$  during NPF in Pallas, Finland (Asmi et al., 2011); and  $700 \text{ W m}^{-2}$  during NPF in Atlanta, USA  
172 (Woo et al., 2001)). The wind speed in summer was lower than in other seasons, as expected from local climatology (Maturilli  
173 et al., 2013). In addition, marine biogenic sources, which provide gaseous precursors (e.g., DMS,  $\text{H}_2\text{SO}_4$ , and  $\text{NH}_3$ ) for  
174 nanoparticle formation, were known as abundant in summer. It was observed that the percentage of air mass passing over high  
175 chlorophyll- $\alpha$  (MODIS data) region, and  $\text{H}_2\text{SO}_4$  and  $\text{NH}_3$  concentrations measured at the site increased in summer (Figure S2  
176 and Table S1 in the Supplement). For example, chlorophyll- $\alpha$  concentration (a proxy for marine phytoplankton biomass) in  
177 the Arctic Ocean surrounding the observation site from 2016 to 2018 began to increase in April and reached a maximum in  
178 May to June (Figure S2 in the Supplement). During the Arctic haze period, the amount of accumulation-mode particles ( $>100$   
179 nm) increased considerably. A significant CS increase occurred in Mar (Figure 2). The high amount of accumulation-mode  
180 particles in spring and the high amount of nucleation-mode particles in summer are consistent with previous findings (Tunved  
181 et al., 2013; Dall’Osto et al., 2017; Heinzenberg et al., 2017).

182 The size distributions of the 3–60 nm particles from 2016 to 2018 (hourly data) were classified into several major  
183 groups using the k-means clustering method. Four distinct clusters were found (Figure 3 (a)), with mode diameters of around  
184 10 nm (cluster 1), 20 nm (cluster 2), 30 nm (cluster 3), and 50 nm (cluster 4). Cluster 1 included newly formed particles with  
185 high population. Cluster 4 had the lowest ultrafine particles concentration, representing the background condition. The  
186 frequencies of each cluster by month are shown in Figure 3 (b). The annual average percentages of each cluster were 7%  
187 (cluster 1), 15% (cluster 2), 23% (cluster 3), and 55% (cluster 4). The frequencies of clusters 1 and 2 increased significantly  
188 and the cluster 2 was often appeared after the cluster 1 in the late spring and summer months (May, June, July, and August),  
189 suggesting that strong particle growth (i.e., increases in mode diameter) after NPF occurred during those months.

190 We identified two distinct types of NPF (Figure 4). In type 1,  $N_{3-25}$  increased significantly with subsequent particle  
191 growth (the freshly formed particles experienced gradual growth), a typical banana-shaped nucleation event, which is regularly  
192 observed at many locations worldwide. In type 2,  $N_{3-25}$  increased significantly without clear subsequent particle growth (almost  
193 no increase of the mode diameter with time, or not clear for growth); this type of event lasted more than 2 hours. Therefore,  
194 the GR could be calculated only for type 1. The cases not matching either of these, they were classified as “undefined” NPF

195 which  $N_{3-25}$  increased for a short period of time (less than 2 hours). This NPF classification approach was similar to methods  
196 employed previously (Dal Maso et al., 2005; Kulmala et al., 2012; Nguyen et al., 2016). The mean occurrence percentage of  
197 NPF days (all types) per year from 2016 to 2018 was 23%. Dall'Osto et al. (2017) found that the average of yearly NPF  
198 occurrence from 2000 to 2010 was 18%, lower than our value, and that this increased over time as the coverage of sea-ice melt  
199 increased. Based on Heintzenberg et al. (2017) study, the mean occurrence percentage of NPF days per year from 2006 to  
200 2015 was estimated to be around 20%. In addition, DMS originating from marine sources can be a key precursor contributing  
201 to NPF in the remote marine atmosphere (Leaitch et al., 2013; Park et al., 2017; Jang et al., 2019). In the Arctic region, the  
202 DMS concentration increased by 33% per decade from 1998 to 2016 (Galí et al., 2019), potentially leading to the increase in  
203 the annual NPF occurrence in this area.

204 It was shown that the concentration of fine particles could be affected by local combustion sources such as local port  
205 and cruise ships (Eckhardt et al., 2013). The effects of anthropogenic sources (e.g., downtown, local port, and cruise ship) on  
206 the NPF were examined by using local wind and air mass trajectory data to find whether air mass or wind passed over the Ny-  
207 Ålesund downtown and local port during NPF events. Also, the concentration of black carbon (BC) at Zeppelin, typically  
208 emitted from primary combustion sources, was used to examine the effect of primary combustion sources on the NPF. We  
209 found that the air mass and wind passed over the downtown including the local port during only two NPF events out of whole  
210 NPF events (170 events). During these two NPF events, the BC concentration little increased. Thus, we believe the effect of  
211 anthropogenic sources on the NPF should be small. Also, in our NPF data analysis we filtered out two NPF events having  
212 increased BC concentration and wind direction coming from the Ny-Ålesund downtown or port.

213 The highest percentage of NPF occurrence for all types was observed in August (63%) and June (61%), followed by  
214 May (47%) and July (42%) as shown in Figure 5. NPF was observed only occasionally in winter during the Arctic night from  
215 November to February, consistent with previous observations (Ström et al., 2009; Heintzenberg et al., 2017). Although NPF  
216 occurrence could be expected to be lowest in April due to highest CS (Figure 2), that was not the case. Our results showed that  
217 NPF occurrence increased significantly in April, was maintained at a high level from May to August, then decreased in  
218 September and October. The average values of CS during NPF event and non-event days were  $0.57 \times 10^{-3} \text{ s}^{-1}$  and  $0.69 \times 10^{-3} \text{ s}^{-1}$ ,  
219 respectively. The higher biological and photochemical activity, lower transport of pollutants from mid-latitudes, and increased  
220 wet scavenging of particles (low CS) in summer likely favored NPF (Ström et al., 2009). In addition, the melting of sea ice in  
221 summer can increase the availability of marine biogenic sources, promoting NPF (Quinn et al., 2008; Tovar-Sánchez et al.,  
222 2010; Dall'Osto et al., 2018). Overall, NPF occurrence is mainly affected by the availability of solar radiation (photochemistry)  
223 and gaseous precursors in addition to the survival probability of clusters or particles (Kulmala et al., 2017). In addition, it was  
224 suggested that fragmentation of primary marine polymer gels, which are derived from phytoplankton along the marginal ice  
225 zone, could be a source for atmospheric nanoparticles (NPF events below 10 nm) in the high Arctic boundary layer  
226 (Heintzenberg et al., 2017; Karl et al., 2019; Mashayekhy Rad et al., 2019).

227 A so-called “weak NPF” event, in which initial formation and growth were completed to  $< 10 \text{ nm}$  without further  
228 growth, was observed. The weak NPF events documented here could not be detected in previous studies where the minimum

229 detectable size was ~10 nm. The fraction of weak NPF occurrences (out of all NPF occurrences each month) was highest in  
230 April (58%) and October (50%), compared to values in May (20%), June (14%), July (8%), August (15%), and September  
231 (25%). In April, this was likely caused by the combination of strong solar radiation (i.e., strong photochemistry for production  
232 of condensing vapors responsible for particle growth) and high CS; in contrast, October's combination of the low solar  
233 radiation (i.e., weak photochemistry) and low CS led to a similar result.

234 NPF lasted for several hours with similar start times (Figure 5). NPF duration was around 6–7 h on average and was  
235 longest in summer. Typically, NPF started between 13:00 and 14:00 (local time), suggesting that photochemical activity with  
236 strong solar radiation played an important role in NPF initiation. The variations in start time from month to month (Mar to  
237 Nov) were smaller than the monthly variations in NPF occurrence or duration. The nighttime NPF also occurred in late fall to  
238 winter (20% out of total NPF events). The exact mechanism for this NPF was unclear. Nanoparticles formed at earlier times  
239 (daytime) in other places may be transported to the site during nighttime (Vehkamaki et al., 2004; Park et al., 2020).

240 Figure 6 shows the MODIS monthly chlorophyll- $\alpha$  concentrations around Svalbard, which increased from April and  
241 decreased after August, consistent with the NPF occurrence frequency. The chlorophyll- $\alpha$  concentration was intense in the  
242 ocean regions southwest and southeast of Svalbard. A recent study revealed that the DMS production capacity of the Greenland  
243 Sea (to the southwest) was 3 times greater than that of the Barents Sea (to the southeast) (Park et al., 2018); this is further  
244 discussed in the context of air mass trajectory data in a later section. Full monthly values of average chlorophyll- $\alpha$  concentration  
245 over the area (70–85°N, 25°W–50°E) and “air mass exposure to chlorophyll- $\alpha$ ” ( $E_{chl}$ ) which explains the DMS mixing ratio of  
246 the air mass arriving at Zeppelin (Park et al., 2018) are summarized in Figure S2 in the Supplement. The  $E_{chl}$  provides the  
247 measure of potential DMS production capacity of the ocean air mass passed over (Park et al., 2018). It was found that “air  
248 mass exposure to chlorophyll- $\alpha$ ” ( $E_{chl}$ ) was correlated well ( $r = 0.69$  and  $p$ -value  $< 0.05$ ; not shown) with the NPF occurrence  
249 frequency, compared to the average chlorophyll- $\alpha$  concentration over the area (70–85°N, 25°W–50°E).

250 To determine the characteristics of particle growth, we calculated the GR in the 3–7 nm, 7–25 nm, and 3–25 nm size  
251 ranges (i.e.,  $GR_{3-7}$ ,  $GR_{7-25}$ , and  $GR_{3-25}$ ) for NPF events (Figure 7). The average  $GR_{3-25}$  for all months was 2.66 nm h<sup>-1</sup>,  
252 comparable to previously reported GR data (0.2–4.1 nm h<sup>-1</sup>) in the Arctic region (Kerminen et al., 2018). The highest monthly  
253 average  $GR_{3-25}$  was observed in July (3.03 nm h<sup>-1</sup>) and the maximum individual value (6.54 nm h<sup>-1</sup>) occurred in June. The  
254 averages of  $GR_{3-7}$  and  $GR_{7-25}$  were 2.07 nm h<sup>-1</sup> and 2.85 nm h<sup>-1</sup>, respectively. However, the GR was much lower than the values  
255 observed in typical urban areas (Table 1), suggesting a lower availability of condensing vapors contributing to particle growth  
256 in the Arctic atmosphere. The formation rates of particles in the same size range as calculated GR were also derived. The  
257 averages of  $J_{3-7}$ ,  $J_{7-25}$ , and  $J_{3-25}$  during NPF events were 0.04 cm<sup>-3</sup> s<sup>-1</sup>, 0.09 cm<sup>-3</sup> s<sup>-1</sup> and 0.12 cm<sup>-3</sup> s<sup>-1</sup>, respectively. The highest  
258 monthly average and maximum for  $J_{3-7}$  were both found in June, but for  $J_{7-25}$  and  $J_{3-25}$  were found in July. The formation rates  
259 (relative standard deviation (RSD) = 39–44%) varied by month more significantly than for GR (RSD = 27–33%). The  
260 formation rates in this study were much lower than those reported in continental areas (Stanier et al., 2004; Hamed et al., 2007;  
261 Wu et al., 2007; Manninen et al., 2010; Xiao et al., 2015; Shen et al., 2016; Cai et al., 2017). A good linear relationship was  
262 found between  $J_{3-7}$  and  $N_{3-7}$  ( $r = 0.97$  and  $p$ -value  $< 0.001$ ) as shown in Figure S3 in the Supplement, indicating that 3–7 nm

263 particles were produced by gas-to-particle conversion rather than direct emissions in the particle phase (i.e., not primary)  
264 (Kalivitis et al., 2019). No significant correlation was found between  $J_{3-7}$  and  $GR_{3-7}$ , suggesting that the vapors participating  
265 in the early stage of NPF could be at least partly different from the vapors contributing to subsequent particle growth (Nieminen  
266 et al., 2014). However, detailed chemical data for nanoparticles during formation and growth should be obtained to achieve  
267 complete understanding of the participating chemical species. Our data indicate that, although NPF occurrence frequency in  
268 the Arctic was comparable to continental areas, the J and GR were much lower. [Time series of daily GR and J in different  
269 modes \( \$GR\_{3-7}\$  and  \$J\_{3-7}\$ , and  \$GR\_{7-25}\$  and  \$J\_{7-25}\$ \), weekly  \$N\_{3-7}\$  and  \$N\_{7-25}\$ , and weekly  \$NH\_3\$  and  \$H\_2SO\_4\$  are shown in Figure S4 in the  
270 Supplement.](#)

271 The existence of significant amounts of nanoparticles as small as 3 nm during NPF events at the study site suggests  
272 that NPF occurred there, rather than the particles being transported from other regions after growth. In other words, if NPF  
273 occurred at other locations far from the study site, the nanoparticles would have grown during transport to the site and few 3  
274 nm particles would have been detected there. [The lifetime of the 3 nm particles in this study \(growth to particles larger than 7  
275 nm\) was estimated to be 2-3 hours on average. It was reported that nanoparticles \(< 5 nm\) in the troposphere could survive for  
276 several hours or less \(Anastasio and Martin, 2001\).](#)

277 Five air mass clusters were found (Figure 8 (a)), representing the contributions of different air masses in different  
278 seasons: clusters 1, 2, 3, 4, and 5 represented southwest (slow), south (slow), southeast (fast), northwest (fast), and northeast  
279 (fast) air masses, respectively. The air mass speed (travel distance/time) was used to determine whether the air mass was slower  
280 or faster compared to the average air mass speed during the measurement period. Cluster 1 dominated in summer, when NPF  
281 occurrence was highest; it had the lowest air mass speed, the lowest fraction of land influence (15%), and the highest fraction  
282 of time spent over the sea (50%) compared to other air mass clusters. Time spent over sea-ice was 35%. [The CS values were  
283  \$0.54 \times 10^{-3} s^{-1}\$ ,  \$0.74 \times 10^{-3} s^{-1}\$ ,  \$0.77 \times 10^{-3} s^{-1}\$ ,  \$0.64 \times 10^{-3} s^{-1}\$ , and  \$0.80 \times 10^{-3} s^{-1}\$  for cluster 1, cluster 2, cluster 3, cluster 4, and cluster  
284 5, respectively., suggesting that cluster 1 had the lowest CS.](#) Our data suggest that a slowly moving air mass, which spent most  
285 of the time over the ocean and sea-ice is the most favourable for NPF.

286 We further explored the potential source regions of the air masses in relation to NPF using air mass backward  
287 trajectory data and the 75<sup>th</sup> percentile of  $N_{3-25}$  (Figure 8 (b)). Increases in the amount of nanoparticles (i.e., NPF events)  
288 occurred more frequently when the air mass passed over the oceanic regions to southwest and south of Svalbard (overall, 49%  
289 of the air mass during NPF was southwest, i.e., cluster 1). As shown earlier (Figure 6), the chlorophyll- $\alpha$  concentration was  
290 strong in the southwest and southeast ocean regions, and the DMS production capacity of the southwest ocean was 3 times  
291 greater than that of the southeast ocean. [The DMS production capacity was defined as the potential amount of DMS produced  
292 from the phytoplankton biomass \(Park et al., 2018\). Several previous studies also support the strong DMS production capacity  
293 in the southwest ocean \(Degerlund and Eilertsen, 2010; Galí and Simó, 2010\).](#) These results suggest that marine biogenic  
294 sources from the southwest ocean (Greenland Sea) region play an important role in NPF in the Arctic.

295 The DMS in the ocean is produced by complicate microbial food-web processes (Stefels et al., 2007). In general,  
296 sea surface DMS maximum occurs following local phytoplankton biomass maxima, thereby leading to lag periods on the order

297 of several weeks to months (so called DMS summer paradox) (Galí and Simó, 2015). This phenomenon could be explained  
298 by several key processes: a succession in phytoplankton composition, grazing by zooplankton on DMSP-containing  
299 phytoplankton and the bacterial degradation of DMSP into DMS (Polimene et al., 2012). However, a clear temporal correlation  
300 between atmospheric (and/or seawater) DMS level and phytoplankton biomass (i.e., chlorophyll- $\alpha$  concentration) has been  
301 observed for the ocean domains where the strong DMS-producer (both containing high intra cellular DMSP content and DMSP  
302 cleavage enzyme) such as haptophytes and dinoflagellates are predominating (e.g., Arnold et al., 2010; Park et al., 2013; Park  
303 et al., 2018; Uhlig et al. 2019; Zhang et al., 2020). Only limited number of phytoplankton class including dinoflagellates and  
304 haptophytes possess enzyme that can convert DMSP into DMS during their growth (Alcolombri et al., 2015). In particular,  
305 *Emiliania huxleyi* and *Phaeocystis sp.* which are highly abundant haptophyte in high latitude oceans play key roles in  
306 controlling global DMS emission because the DMS production capacity of these species is much higher than other globally  
307 abundant phytoplankton species (Liss et al., 1994; McParland and Levine, 2019). For example, multi-year measurements of  
308 atmospheric DMS mixing ratios at Zeppelin station showed a strong correlation between sea-surface chlorophyll- $\alpha$   
309 concentration (estimated by MODIS-aqua) and atmospheric DMS levels (Park et al., 2013; Park et al., 2018). Furthermore,  
310 relationships between the atmospheric DMS and phytoplankton biomass were regionally and temporally varied with the  
311 relative abundance of strong DMS(P)-producer (Park et al., 2018). This is because the oceanic DMS production in vicinity of  
312 the observation site (i.e., Greenland and Barents Seas) largely governed by direct DMS exudation of phytoplankton that has  
313 both high cellular DMSP content and DMSP-cleavage enzyme during phytoplankton bloom period. Recent study conducted  
314 at remote Antarctic site also revealed that the number concentration of nano-size particles (3–10 nm in diameter) was positively  
315 correlated with the chlorophyll- $\alpha$  concentration during the period when strong DMS-producer predominate (dominance of  
316 *Phaeocystis* > 50%; estimated by PHYSAT algorithm) (Jang et al., 2019).

317 We then examined the chemical characteristics of particulate matter (PM) and daily concentration of gaseous  $\text{NH}_3$ .  
318 The seasonal characteristics of ionic species ( $\text{Na}^+$ ,  $\text{Mg}^{2+}$ ,  $\text{K}^+$ ,  $\text{NH}_4^+$ ,  $\text{NO}_3^-$ ,  $\text{SO}_4^{2-}$ , and  $\text{Cl}^-$ ) in PM from 2016 to 2018 (Table S1  
319 in the Supplement) revealed that the contributions of primary sea salt particles ( $\text{Na}^+$ ,  $\text{Mg}^{2+}$ , and  $\text{Cl}^-$ ) increased in winter with  
320 high wind speeds, while the contributions of  $\text{NH}_4^+$ ,  $\text{NO}_3^-$ , and  $\text{SO}_4^{2-}$  (secondary species) increased in spring and summer. The  
321 slope of the cation equivalents ( $\text{Na}^+$ ,  $\text{Mg}^{2+}$ ,  $\text{K}^+$ , and  $\text{NH}_4^+$ ) versus the anion equivalents ( $\text{NO}_3^-$ ,  $\text{SO}_4^{2-}$ , and  $\text{Cl}^-$ ) (= 0.98; not  
322 shown) suggested that the measured cations were mostly neutralized by the anions (Zhang et al., 2015). These ionic species  
323 can exist in large particles, and do not necessarily represent the chemical composition of the nanoparticles, but they can provide  
324 information about the overall chemical properties of the particles in different seasons. The non-sea salt sulfate ( $\text{nss-SO}_4^{2-}$ )  
325 could have had a secondary origin from the DMS from the sea (Park et al., 2017; Kecorius et al., 2019). The  $\text{SO}_4^{2-}$  could also  
326 come from sea salt particles (primary production of  $\text{SO}_4^{2-}$ ) (Karl et al., 2019). Thus, the concentration of  $\text{nss-SO}_4^{2-}$  was derived  
327 from  $\text{nss-SO}_4^{2-}$  ( $\mu\text{g m}^{-3}$ ) = total  $\text{SO}_4^{2-}$  ( $\mu\text{g m}^{-3}$ ) –  $0.252 \times \text{Na}^+$  ( $\mu\text{g m}^{-3}$ ) by using the measured  $\text{SO}_4^{2-}$  and  $\text{Na}^+$  concentrations (Zhan  
328 et al., 2017). The  $\text{nss-SO}_4^{2-}$  ratio ( $\text{nss-SO}_4^{2-}/\text{total SO}_4^{2-}$ ) was significantly higher on NPF event days than on non-event days  
329 ( $p$ -value < 0.01; Figure 9). The  $\text{NH}_3$  concentration was higher on NPF event days than on non-event days as shown in Figure  
330 9 ( $p$ -value < 0.001), similar to results shown in Dall’Osto et al. (2017), although daily  $\text{NH}_3$  concentration was not significantly

331 correlated with the  $N_{3-25}$  as shown in Figure S5 in the Supplement. The  $NH_3$  in the Arctic can originate from biological and  
332 animal sources (e.g., seabird colonies) (Tovar-Sánchez et al., 2010; Croft et al., 2016; Dall’Osto et al., 2017). The  $SO_2$  was not  
333 significantly higher on NPF event days than on non-event days (Figure 9), and not significantly correlated with the  $N_{3-25}$   
334 (Figure S5 in the Supplement). On the other hand, the  $H_2SO_4$  was found to be higher on the NPF event days (Figure 9) and  
335 was correlated with the  $N_{3-25}$  (Figure S5 in the Supplement), suggesting that the  $H_2SO_4$  should play an important role in  
336 nucleation and growth. Our data were limited to fully explain the nucleation mechanism. Further studies should be required to  
337 elucidate the nucleation mechanism by directly measuring chemical composition of nanoparticles and various precursor vapors.

338 The NPF event probability distribution with daily CS and temperature was included in Figure S6 in the Supplement.  
339 The NPF event probability was calculated by the ratio of the NPF event days per total days for the given CS and temperature.  
340 The NPF event probability increased at moderate temperatures when the CS was low, while when the CS was high, the  
341 probability increased at relatively high temperature as shown in Figure S6 in the Supplement.

342 We calculated the NPF criterion ( $L_T$ ) values for NPF event and non-event days (Figure 10). The seven non-event  
343 days when GR could be obtained from pre-existing aerosols were selected for the calculation of the  $L_T$  (Kuang et al., 2010).  
344 The NPF duration time was determined using the proposed method (Kulmala et al., 2012), with the time range of non-event  
345 days set as daytime (06:00–18:00). When NPF occurred, the  $L_T$  ranged from 0.003–0.27 with a mean and median of 0.044 and  
346 0.041, respectively; all values were less than 1. The  $L_T$  values of non-event days ranged from 0.34–2.59 with a mean and a  
347 median of 1.49 and 1.61, respectively; five days were larger than 1. These observations were consistent with previous studies  
348 of NPF events in clean or moderately-polluted areas (Tecamac, Atlanta, Boulder, and Hyytiälä), ranging from 0.0075–0.66  
349 (Kuang et al., 2010), and in a highly-polluted area (Beijing), ranging from 0.22–1.75 (Cai et al., 2017). Our data suggest that  
350  $L_T$  can also be useful for determining the occurrence of NPF in the Arctic, but not at 100% certainty. Uncertainties in  $H_2SO_4$   
351 concentration inferred from daily  $SO_2$  data (as discussed in the experimental section) and other parameters such as the  
352 measured GR and averaging time for  $L_T$  (i.e., NPF duration time) could contribute to unclear separation of NPF event and non-  
353 event days (Figure 10).

#### 354 4 Conclusions

355 We examined the characteristics of Arctic NPF at the Mount Zeppelin site by conducting continuous measurements  
356 of nanoparticles down to 3 nm size from 2016 to 2018. The size distributions of 3–60 nm particles were classified into distinct  
357 clusters with strong seasonal variability and mode diameters of 10 nm (cluster 1), 20 nm (cluster 2), 30 nm (cluster 3), and 50  
358 nm (cluster 4). A significant number of nanoparticles as small as 3 nm often appeared during NPF, particularly in summer,  
359 suggesting that there is a good chance that these were produced near the site rather than being transported from other regions  
360 after growth. The average NPF occurrence frequency per year was 23%.  $J_{3-7}$  averaged  $0.04 \text{ cm}^3 \text{ s}^{-1}$ , ranging from 0.001–0.54  
361  $\text{cm}^3 \text{ s}^{-1}$ , and  $GR_{3-7}$  averaged  $2.07 \text{ nm h}^{-1}$ , ranging from 0.29–5.17  $\text{nm h}^{-1}$ . These data suggest that the NPF occurrence frequency  
362 in the Arctic is comparable to those in continental areas although the  $J$  and  $GR$  were lower in the Arctic. We next identified



363 five major air mass clusters using backward trajectory analysis; PSCF results indicated that air masses from the south and  
364 southwest ocean regions were related to the elevated concentrations of nanoparticles at the site. This region was consistent  
365 with elevated chlorophyll- $\alpha$  and DMS production capacity, suggesting that marine biogenic sources should play an important  
366 role in Arctic NPF. The concentrations of  $\text{NH}_3$  and  $\text{H}_2\text{SO}_4$  were higher on NPF event days than on non-event days. Previously  
367 developed NPF criteria (a low ratio of loss rate to growth rate of clusters favors NPF) were applicable to Arctic NPF occurrence.  
368

369 *Acknowledgements.* This research was supported by a National Research Foundation of Korea Grant from the Korean  
370 Government (Ministry of Science and ICT) (NRF-2016M1A5A1901779) (KOPRI-PN20081) (Title: Circum Arctic Permafrost  
371 Environment Change Monitoring, Future Prediction and Development Techniques of Useful Biomaterials (CAPEC Project)),  
372 a National Leading Research Laboratory program (NPF-2019R1A2C3007202) and Samsung Advanced Institute of  
373 Technology. We also would like to thank research engineers Tabea Henning, Ondrej Tesar, and Birgitta Noone from ACES  
374 and the staff from the Norwegian Polar Institute (NPI) for their on-site support. NPI is also acknowledged for substantial long-  
375 term support in maintaining the measurements at Zeppelin Observatory. This work was financially supported by the long-term  
376 support of the Swedish EPA's (Naturvårdsverket) Environmental monitoring program (Miljöövervakning), the Knut-and-  
377 Alice-Wallenberg Foundation within the ACAS project (Arctic Climate Across Scales, project no. 2016.0024) and FORMAS  
378 (Project # 2016-01427).

379  
380 *Data availability.* The nano-SMPS data (3–60 nm) are available in Korea Polar Data Center (KPDC) web site  
381 ('<https://kpdc.kopri.re.kr/search/>'), and the raw data can be distributed upon request to the corresponding author  
382 ([kpark@gist.ac.kr](mailto:kpark@gist.ac.kr)). The DMPS (5–810 nm and 10–790 nm) data are available in Stockholm University and Norwegian  
383 Institute for Air Research (NILU). The meteorological data for solar radiation (SRAD) were provided by the Alfred Wegener  
384 Institute (Maturilli, 2019).

385  
386 *Competing interests.* The authors declare that they have no conflict of interest.  
387

## 388 **References**

- 389 Aas, W., M. Fiebig, S., Solberg and K. E. Yttri.: Monitoring of long-range transported air pollutants in Norway. Annual report  
390 2018, NILU rapport, 2019.
- 391 Alcolombri, U., Ben-Dor, S., Feldmesser, E., Levin, Y., Tawfik, D. S., and Vardi, A.: Identification of the algal dimethyl  
392 sulfide-releasing enzyme: a missing link in the marine sulfur cycle, *Science*, 348, 1466–1469,  
393 <https://doi.org/10.1126/science.aab1586>, 2015.

394 Anastasio, C. and Martin, S. T.: Atmospheric Nanoparticles, *Rev. Mineral. Geochem.*, 44 (1), 293-349,  
395 <http://doi.org/10.2138/rmg.2001.44.08>, 2001.

396 Arnold, S. R., Spracklen, D. V., Gebhardt, S., Custer, T., Williams, J., Peeken, I., and Alvain, S.: Relationships between  
397 atmospheric organic compounds and air-mass exposure to marine biology, *Environ. Chem.*, 7(3), 232-241,  
398 <https://dx.doi.org/10.1071/EN09144>, 2010

399 Asmi, E., Kivekäs, N., Kerminen, V. M., Komppula, M., Hyvärinen, A. P., Hatakka, J., Viisanen, Y., and Lihavainen, H.:  
400 Secondary new particle formation in Northern Finland Pallas site between the years 2000 and 2010, *Atmos. Chem. Phys.*,  
401 11 (24), 12959-12972, <https://doi.org/10.5194/acp-11-12959-2011>, 2011

402 Asmi, E., Kondratyev, V., Brus, D., Laurila, T., Lihavainen, H., Backman, J., Vakkari, V., Aurela, M., Hatakka, J., Viisanen,  
403 Y., Uttal, T., Ivakhov, V., and Makshtas, A.: Aerosol size distribution seasonal characteristics measured in Tiksi, Russian  
404 Arctic, *Atmos. Chem. Phys.*, 16 (3), 1271-1287, <https://doi.org/10.5194/acp-16-1271-2016>, 2016.

405 Beddows, D. C., Dall'Osto, M., and Harrison, R. M.: Cluster analysis of rural, urban, and curbside atmospheric particle size  
406 data, *Environ. Sci. Technol.*, 43 (13), 4694-4700, <https://doi.org/10.1021/es803121t>, 2009.

407 Beine, H., Argentini, S., Maurizi, A., Mastrantonio, G., and Viola, A.: The local wind field at Ny-Ålesund and the Zeppelin  
408 mountain at Svalbard, *Meteorol. Atmos. Phys.*, 78 (1-2), 107-113, <https://doi.org/10.1007/s007030170009>, 2001.

409 Cai, R., Yang, D., Fu, Y., Wang, X., Li, X., Ma, Y., Hao, J., Zheng, J., and Jiang, J.: Aerosol surface area concentration: A  
410 governing factor in new particle formation in Beijing, *Atmos. Chem. Phys.*, 17 (20), 12327-12340,  
411 <https://doi.org/10.5194/acp-17-12327-2017>, 2017.

412 Covert, D. S., Wiedensohler, A., Aalto, P., Heintzenberg, J., McMurry, P. H., and Leck, C.: Aerosol number size distributions  
413 from 3 to 500 nm diameter in the arctic marine boundary layer during summer and autumn, *Tellus Ser. B-Chem. Phys.*  
414 *Meteorol.*, 48 (2), 197-212, <https://doi.org/10.3402/tellusb.v48i2.15886>, 1996.

415 Croft, B., Martin, R. V., Leaitch, W. R., Tunved, P., Breider, T. J., D'Andrea, S. D., and Pierce, J. R.: Processes controlling  
416 the annual cycle of Arctic aerosol number and size distributions, *Atmos. Chem. Phys.*, 16 (6), 3665-3682,  
417 <https://doi.org/10.5194/acp-16-3665-2016>, 2016.

418 Dal Maso, M., Kulmala, M., Riipinen, I., Wagner, R., Hussein, T., Aalto, P. P., and Lehtinen, K. E.: Formation and growth of  
419 fresh atmospheric aerosols: eight years of aerosol size distribution data from SMEAR II, Hyytiälä, Finland, *Boreal*  
420 *Environ. Res.*, 10 (5), 323-336, 2005.

421 Dall'Osto, M., Beddows, D. C. S., Tunved, P., Krejci, R., Strom, J., Hansson, H. C., Yoon, Y. J., Park, K. T., Becagli, S.,  
422 Udisti, R., Onasch, T., CD, O. D., Simo, R., and Harrison, R. M.: Arctic sea ice melt leads to atmospheric new particle  
423 formation, *Sci. Rep.*, 7 (1), 3318, <https://doi.org/10.1038/s41598-017-03328-1>, 2017.

424 Dall'Osto, M., Geels, C., Beddows, D. C. S., Boertmann, D., Lange, R., Nojgaard, J. K., Harrison, R. M., Simo, R., Skov, H.,  
425 and Massling, A.: Regions of open water and melting sea ice drive new particle formation in North East Greenland, *Sci.*  
426 *Rep.*, 8 (1), 6109, <https://doi.org/10.1038/s41598-018-24426-8>, 2018.



427 Degerlund, H. and Eilertsen, H. C.: Main Species Characteristics of Phytoplankton Spring Blooms in NE Atlantic and Arctic  
428 Waters (68-80°N), *Estuaries Coasts*, 33, 242-269, <http://dx.doi.org/10.1007/s12237-009-9167-7>, 2010.

429 Eckhardt, S., Hermansen, O., Grythe, H., Fiebig, M., Stebel, K., Cassiani, M., Baecklund, A., and Stohl, A.: The influence of  
430 cruise ship emissions on air pollution in Svalbard a harbinger of a more polluted Arctic? *Atmos. Chem. Phys.*, 13, 8401-  
431 8409, <https://doi.org/10.5194/acp-13-8401-2013>, 2013.

432 EMEP/CCC: Manual for sampling and chemical analysis, Norwegian Institute for Air Research, Kjeller, EMEP/CCC Report  
433 1/95 (Last rev. 2001), <http://tarantula.nilu.no/projects/ccc/>, 2001.

434 Fleming, Z. L., Monks, P. S., and Manning, A. J.: Untangling the influence of air-mass history in interpreting observed  
435 atmospheric composition, *Atmos. Res.*, 104, 1-39, <https://doi.org/10.1016/j.atmosres.2011.09.009>, 2012.

436 Gao, J., Chai, F., Wang, T., and Wang, W.: Particle number size distribution and new particle formation (NPF) in Lanzhou,  
437 Western China, *Particuology*, 9 (6), 611-618, <https://doi.org/10.1016/j.partic.2011.06.008>, 2011.

438 Galí, M. and Simó R.: Occurrence and cycling of dimethylated sulfur compounds in the Arctic during summer receding of the  
439 ice edge, *Mar. Chem.*, 122 (1-4), 105-117, <https://doi.org/10.1016/j.marchem.2010.07.003>, 2010.

440 Galí, M. and Simó R.: A metaanalysis of oceanic DMS and DMSP cycling processes: Disentangling the summer paradox,  
441 *Global Biogeochem. Cycles*, 29, 496-515, <https://doi.org/10.1002/2014GB004940>, 2015.

442 Galí, M., Devred, E., Babin, M., and Levasseur, M.: Decadal increase in Arctic dimethylsulfide emission, *Proc. Natl. Acad.*  
443 *Sci. U. S. A.*, 116 (39), 19311-19317, <https://doi.org/10.1073/pnas.1904378116>, 2019.

444 Giamarelou, M., Eleftheriadis, K., Nyeki, S., Tunved, P., Torseth, K., and Biskos, G.: Indirect evidence of the composition of  
445 nucleation mode atmospheric particles in the high Arctic, *J. Geophys. Res. Atmos.*, 121, 965-975,  
446 <https://doi.org/10.1002/2015JD023646>, 2016.

447 Gong, Y., Hu, M., Cheng, Y., Su, H., Yue, D., Liu, F., Wiedensohler, A., Wang, Z., Kalesse, H., Liu, S., Wu, Z., Xiao, Z., Mi,  
448 P., and Zhang, Y.: Competition of coagulation sink and source rate: New particle formation in the Pearl River Delta of  
449 China, *Atmos. Environ.*, 44, 3278-3285, <https://doi.org/10.1016/j.atmosenv.2010.05.049>, 2010.

450 Hamed, A., Joutsensaari, J., Mikkonen, S., Sogacheva, L., Maso, M. D., Kulmala, M., Cavalli, F., Fuzzi, S., Facchini, M., and  
451 Decesari, S.: Nucleation and growth of new particles in Po Valley, Italy, *Atmos. Chem. Phys.*, 7 (2), 355-376,  
452 <https://doi.org/10.5194/acp-7-355-2007>, 2007.

453 Heintzenberg, J., Leck, C., and Tunved, P.: Potential source regions and processes of the aerosol in the summer Arctic, *Atmos.*  
454 *Chem. Phys.*, 15 (6), 6487-6502, <https://doi.org/10.5194/acp-15-6487-2015>, 2015.

455 Heintzenberg, J., Tunved, P., Galí, M., and Leck, C.: New particle formation in the Svalbard region 2006-2015, *Atmos. Chem.*  
456 *Phys.*, 17 (10), 6153-6175, <https://doi.org/10.5194/acp-17-6153-2017>, 2017.

457 Hirdman, D., Burkhardt, J. F., Sodemann, H., Eckhardt, S., Jefferson, A., Quinn, P. K., Sharma, S., Ström, J., and Stohl, A.:  
458 Long-term trends of black carbon and sulphate aerosol in the Arctic: changes in atmospheric transport and source region  
459 emissions, *Atmos. Chem. Phys.*, 10 (19), 9351-9368, <https://doi.org/10.5194/acp-10-9351-2010>, 2010.

460 Hussein, T., Dal Maso, M., Petaja, T., Koponen, I. K., Paatero, P., Aalto, P. P., Hameri, K., and Kulmala, M.: Evaluation of  
461 an automatic algorithm for fitting the particle number size distributions, *Boreal Environ. Res.*, 10 (5), 337-355, 2005.

462 Iziomon, M., Lohmann, U., and Quinn, P.: Summertime pollution events in the Arctic and potential implications, *J. Geophys.*  
463 *Res. Atmos.*, 111, D12206, <https://doi.org/10.1029/2005JD006223>, 2006.

464 Jang, E., Park, K.-T., Yoon, Y. J., Kim, T.-W., Hong, S.-B., Becagli, S., Traversi, R., Kim, J., and Gim, Y.: New particle  
465 formation events observed at the King Sejong Station, Antarctic Peninsula – Part 2: Link with the oceanic biological  
466 activities, *Atmos. Chem. Phys.*, 19, 7595-7608, <https://doi.org/10.5194/acp-19-7595-2019>, 2019

467 Järvinen, E., Virkkula, A., Nieminen, T., Aalto, P. P., Asmi, E., Lanconelli, C., Busetto, M., Lupi, A., Schioppo, R., Vitale,  
468 V., Mazzola, M., Petäjä, T., Kerminen, V. M., and Kulmala, M.: Seasonal cycle and modal structure of particle number  
469 size distribution at Dome C, Antarctica, *Atmos. Chem. Phys.*, 13 (15), 7473-7487, [https://doi.org/10.5194/acp-13-7473-](https://doi.org/10.5194/acp-13-7473-2013)  
470 [2013](https://doi.org/10.5194/acp-13-7473-2013), 2013.

471 Jeffries, M. and Richter-Menge, J.: State of the climate in 2011: The Arctic., *Bull. Am. Meteorol. Soc.*, 93, S127-S148,  
472 <https://doi.org/10.1175/2012BAMSStateoftheClimate.1>, 2012.

473 Kalivitis, N., Kerminen, V.-M., Kouvarakis, G., Stavroulas, I., Tzitzikalaki, E., Kalkavouras, P., Daskalakis, N.,  
474 Myriokefalitakis, S., Bougiatioti, A., Manninen, H. E., Roldin, P., Petäjä, T., Boy, M., Kulmala, M., Kanakidou, M., and  
475 Mihalopoulos, N.: Formation and growth of atmospheric nanoparticles in the eastern Mediterranean: Results from long-  
476 term measurements and process simulations, *Atmos. Chem. Phys.*, 19 (4), 2671-2686, [https://doi.org/10.5194/acp-19-](https://doi.org/10.5194/acp-19-2671-2019)  
477 [2671-2019](https://doi.org/10.5194/acp-19-2671-2019), 2019.

478 Karl, M., Leck, C., Coz, E., and Heintzenberg, J.: Marine nanogels as a source atmospheric nanoparticles in the high Arctic,  
479 *Geophys. Res. Lett.*, 40, 3738-374., <https://doi.org/10.1002/grl.50661>, 2013.

480 Karl, M., Leck, C., Mashayekhy Rad, F., Bäcklund, A., Lopez-Aparicio, S., and Heintzenberg, J.: New insights in sources of  
481 the sub-micrometre aerosol at Mt. Zeppelin observatory (Spitsbergen) in the year 2015, *Tellus Ser. B-Chem. Phys.*  
482 *Meteorol.*, 71:1, 1613143, <https://doi.org/10.1080/16000889.2019.1613143>, 2019.

483 Kecorius S., Vogl, T., Paasonen, P., Lampilahti, J., Rothenberg, D., Wex, H., Zeppenfeld, S., van Pinxteren, M., Hartmann,  
484 M., Henning, S., Gong, X., Welti, A., Kulmala, M., Stratmann, F., Herrmann, H., and Wiedensohler, A.: New particle  
485 formation and its effect on cloud condensation nuclei abundance in the summer Arctic: a case study in the Fram Strait and  
486 Barents Sea, *Atmos. Chem. Phys.*, 19, 14339-14364, <https://doi.org/10.5194/acp-19-14339-2019>, 2019.

487 Kerminen, V.-M., Chen, X., Vakkari, V., Petäjä, T., Kulmala, M., and Bianchi, F.: Atmospheric new particle formation and  
488 growth: review of field observations, *Environ. Res. Lett.*, 13 (10), <https://doi.org/10.1088/1748-9326/aadf3c>, 2018.

489 Kuang, C., Riipinen, I., Sihto, S. L., Kulmala, M., McCormick, A. V., and McMurry, P. H.: An improved criterion for new  
490 particle formation in diverse atmospheric environments, *Atmos. Chem. Phys.*, 10 (17), 8469-8480,  
491 <https://doi.org/10.5194/acp-10-8469-2010>, 2010.

492 Kuang, C., Chen, M., Zhao, J., Smith, J., McMurry, P. H., and Wang, J.: Size and time-resolved growth rate measurements of  
493 1 to 5 nm freshly formed atmospheric nuclei, *Atmos. Chem. Phys.*, 12 (7), 3573-3589, [https://doi.org/10.5194/acp-12-](https://doi.org/10.5194/acp-12-3573-2012)  
494 [3573-2012](https://doi.org/10.5194/acp-12-3573-2012), 2012.

495 Kulmala, M., Vehkamäki, H., Petäjä, T., Dal Maso, M., Lauri, A., Kerminen, V. M., Birmili, W., and McMurry, P. H.:  
496 Formation and growth rates of ultrafine atmospheric particles: a review of observations, *J. Aerosol Sci.*, 35 (2), 143-176,  
497 <https://doi.org/10.1016/j.jaerosci.2003.10.003>, 2004.

498 Kulmala, M., Petaja, T., Nieminen, T., Sipila, M., Manninen, H. E., Lehtipalo, K., Dal Maso, M., Aalto, P. P., Junninen, H.,  
499 Paasonen, P., Riipinen, I., Lehtinen, K. E., Laaksonen, A., and Kerminen, V. M.: Measurement of the nucleation of  
500 atmospheric aerosol particles, *Nature Protocols*, 7 (9), 1651-1667, <https://doi.org/10.1038/nprot.2012.091>, 2012.

501 Kulmala, M., Kerminen, V. M., Petaja, T., Ding, A. J., and Wang, L.: Atmospheric gas-to-particle conversion: why NPF events  
502 are observed in megacities?, *Faraday Discuss*, 200, 271-288, <https://doi.org/10.1039/C6FD00257A>, 2017.

503 Law, K. S. and Stohl, A.: Arctic air pollution: Origins and impacts, *Science*, 315 (5818), 1537-1540, [https://doi.org/](https://doi.org/10.1126/science.1137695)  
504 [10.1126/science.1137695](https://doi.org/10.1126/science.1137695), 2007.

505 Leaitch, W. R., Sharma, S., Huang, L., Toom-Saunty, D., Chivulescu, A., Macdonald, A. M., von Salzen, K., Pierce, J. R.,  
506 Bertram, A. K., and Schroder, J. C.: Dimethyl sulfide control of the clean summertime Arctic aerosol and cloud, *Elem.*  
507 *Sci. Anth.*, 1, <http://doi.org/10.12952/journal.elementa.000017>, 2013.

508 Liss, P.S., Malin, G., Turner, S.M., and Holligan, P.M., Dimethyl sulphide and Phaeocystis: a review, *J. Mar. Syst.*, 5 (1), 41–  
509 [53, https://doi.org/10.1016/0924-7963\(94\)90015-9](https://doi.org/10.1016/0924-7963(94)90015-9), 1994.

510 Manninen, H. E., Nieminen, T., Asmi, E., Gagné, S., Häkkinen, S., Lehtipalo, K., Aalto, P., Vana, M., Mirme, A., Mirme, S.,  
511 Hörrak, U., Plass-Dülmer, C., Stange, G., Kiss, G., Hoffer, A., Törő, N., Moerman, M., Henzing, B., de Leeuw, G.,  
512 Brinkenberg, M., Kouvarakis, G. N., Bougiatioti, A., Mihalopoulos, N., and Dowd, C., Ceburnis, D., Arneth, A.,  
513 Svenningsson, B., Swietlicki, E., Tarozzi, L., Decesari, S., Facchini, M. C., Birmili, W., Sonntag, A., Wiedensohler, A.,  
514 Boulon, J., Sellegri, K., Laj, P., Gysel, M., Bukowiecki, N., Weingartner, E., Wehrle, G., Laaksonen, A., Hamed, A.,  
515 Joutsensaari, J., Petäjä, T., Kerminen, V. M., and Kulmala, M.: EUCAARI ion spectrometer measurements at 12 European  
516 sites – analysis of new particle formation events, *Atmos. Chem. Phys.*, 10 (16), 7907-7927, [https://doi.org/10.5194/acp-](https://doi.org/10.5194/acp-10-7907-2010)  
517 [10-7907-2010](https://doi.org/10.5194/acp-10-7907-2010), 2010.

518 Maturilli, M., Herber, A., and König-Langlo, G.: Climatology and time series of surface meteorology in Ny-Ålesund, Svalbard,  
519 *Earth System Science Data*, 5, 155-163, <https://doi.org/10.5194/essd-5-155-2013>, 2013.

520 Maturilli, M.: Basic and other measurements of radiation and continuous meteorological observations at station Ny-Ålesund  
521 (2016-2018), reference list of 72 datasets. Alfred Wegener Institute - Research Unit Potsdam, PANGAEA,  
522 <doi.pangaea.de/10.1594/PANGAEA.908444>, 2019.

523 Mashayekhy Rad, F., Zurita, J., Gilles, P., Rutgeerts, L. A. J., Nilsson, U., Ilag, L. L., and Leck, C.: Measurements of  
524 Atmospheric Proteinaceous Aerosol in the Arctic Using a Selective UHPLC/ESI-MS/MS Strategy, *J. Am. Soc. Mass*  
525 *Spectrom.*, 30(1), 161-173, <https://doi.org/10.1007/s13361-019-02137-2>, 2019.

526 McParland, E. L. and Levine, N. M.: The role of differential DMSP production and community composition in predicting  
527 variability of global surface DMSP concentrations. *Limnol. Oceanogr.*, 64, 757–773, <https://doi.org/10.1002/lno.11076>,  
528 2019.

529 McMurry, P. H., Fink, M., Sakurai, H., Stolzenburg, M. R., Mauldin, R. L., Smith, J., Eisele, F., Moore, K., Sjostedt, S.,  
530 Tanner, D., Huey, L. G., Nowak, J. B., Edgerton, E., and Voisin, D.: A criterion for new particle formation in the sulfur-  
531 rich Atlanta atmosphere, *J. Geophys. Res.*, 110, <https://doi.org/10.1029/2005JD005901>, 2005.

532 Merikanto, J., Spracklen, D., Mann, G., Pickering, S., and Carslaw, K.: Impact of nucleation on global CCN, *Atmos. Chem.*  
533 *Phys.*, 9 (21), 8601-8616, <https://doi.org/10.5194/acp-9-8601-2009>, 2009.

534 Mikkonen, S., Romakkaniemi, S., Smith, J. N., Korhonen, H., Petäjä, T., Plass-Duelmer, C., Boy, M., McMurry, P. H.,  
535 Lehtinen, K. E. J., Joutsensaari, J., Hamed, A., Mauldin Iii, R. L., Birmili, W., Spindler, G., Arnold, F., Kulmala, M., and  
536 Laaksonen, A.: A statistical proxy for sulphuric acid concentration, *Atmos. Chem. Phys.*, 11 (7), 20141-20179,  
537 <https://doi.org/10.5194/acp-11-11319-2011>, 2011.

538 Neuber, R., Ström, J., Hübner, C., Hermansen, O., Arya, B. C., Beichen, Z., Kallenborn, R., Karasinki, G., Ivanov, B., and  
539 Moen, J.: Atmospheric research in Ny-Ålesund-a flagship programme, Norsk Polarinstitut, 2011.

540 Nguyen, Q. T., Glasius, M., Sørensen, L. L., Jensen, B., Skov, H., Birmili, W., Wiedensohler, A., Kristensson, A., Nøjgaard,  
541 J. K., and Massling, A.: Seasonal variation of atmospheric particle number concentrations, new particle formation and  
542 atmospheric oxidation capacity at the high Arctic site Villum Research Station, Station Nord, *Atmos. Chem. Phys.*, 16  
543 (17), 11319-11336, <https://doi.org/10.5194/acp-16-11319-2016>, 2016.

544 Nieminen, T., Asmi, A., Dal Maso, M., Aalto, P. P., Keronen, P., Petäjä, T., Kulmala, M., and Kerminen, V.-M.: Trends in  
545 atmospheric new-particle formation: 16 years of observations, *Boreal Environ. Res.*, 19, 191-214, 2014.

546 O'Neill, N., Pancrati, O., Baibakov, K., Eloranta, E., Batchelor, R., Freemantle, J., McArthur, L., Strong, K., and Lindenmaier,  
547 R.: Occurrence of weak, sub-micron, tropospheric aerosol events at high Arctic latitudes, *Geophys. Res. Lett.*, 35 (14),  
548 L14814, <https://doi.org/10.1029/2008GL033733>, 2008.

549 Park, K.-T., Lee, K., Yoon, Y.-J., Lee, H.-W., Kim, H.-C., and Lee, B.-Y., Hermansen, O., Kim, T.-W., Holmén, K.: Linking  
550 atmospheric dimethyl sulphide and the Arctic Ocean spring bloom, *Geophys. Res. Lett.*, 40, 155-160,  
551 <https://doi.org/10.1029/2012GL054560>, 2013.

552 Park, K.-T., Jang, S., Lee, K., Yoon, Y. J., Kim, M.-S., Park, K., Cho, H.-J., Kang, J.-H., Udisti, R., and Lee, B.-Y.:  
553 Observational evidence for the formation of DMS-derived aerosols during Arctic phytoplankton blooms, *Atmos. Chem.*  
554 *Phys.*, 17 (15), 9665-9675, <https://doi.org/10.5194/acp-17-9665-2017>, 2017.

555 Park, K. T., Lee, K., Kim, T. W., Yoon, Y. J., Jang, E. H., Jang, S., and Lee, B. Y., Hermansen, O.: Atmospheric DMS in the  
556 Arctic Ocean and its relation to phytoplankton biomass, *Glob. Biogeochem. Cycles*, 32 (3), 351-359,  
557 <https://doi.org/10.1002/2017GB005805>, 2018.

558 Park, J., Dall'Osto, M., Park, K., Gim, Y., Kang, H. J., Jang, E., Park, K.-T., Park, M., Yum, S. S., Jung, J., Lee, B. Y., and  
559 Yoon, Y. J.: Shipborne observations reveal contrasting Arctic marine, Arctic terrestrial and Pacific marine aerosol  
560 properties, *Atmos. Chem. Phys.*, 20, 5573-5590, <https://doi.org/10.5194/acp-20-5573-2020>, 2020.

561 Pekney, N. J., Davidson, C. I., Zhou, L., and Hopke, P. K.: Application of PSCF and CPF to PMF-modeled sources of PM<sub>2.5</sub>  
562 in Pittsburgh, *Aerosol Sci. Technol.*, 40 (10), 952-961, <https://doi.org/10.1080/02786820500543324>, 2007.

563 Polimene, L., Archer, S. D., Butenschön, M., Allen, J. I.: A mechanistic explanation of the Sargasso Sea DMS “summer  
564 paradox”, *Biogeochemistry*, 110, 243–255, <https://doi.org/10.1007/s10533-011-9674-z>, 2012.

565 Quinn, P., Miller, T., Bates, T., Ogren, J., Andrews, E., and Shaw, G.: A 3-year record of simultaneously measured aerosol  
566 chemical and optical properties at Barrow, Alaska, *J. Geophys. Res: Atmospheres*, 107 (D11), 4130,  
567 <https://doi.org/10.1029/2001JD001248>, 2002.

568 Quinn, P., Shaw, G., Andrews, E., Dutton, E., Ruoho-Airola, T., and Gong, S.: Arctic haze: current trends and knowledge gaps,  
569 *Tellus Ser. B-Chem. Phys. Meteorol.*, 59 (1), 99-114, <https://doi.org/10.1111/j.1600-0889.2006.00238.x>, 2007.

570 Quinn, P., Bates, T., Baum, E., Bond, T., Doubleday, N., Fiore, A. M., Flanner, M., Fridlind, A., Garrett, T. J., Koch, D.,  
571 Menon, S., Shindell, D., Stohl, A., and Warren, S. G.: Short-Lived Pollutants in the Arctic: their climate impact and  
572 possible mitigation strategies, *Atmos. Chem. Phys.*, 8, 1723-1735, <https://doi.org/10.5194/acp-8-1723-2008>, 2008.

573 Radke, L. F., Lyons, J. H., Hegg, D. A., Hobbs, P. V., and Bailey, I. H.: Airborne observations of Arctic aerosols. I:  
574 Characteristics of Arctic haze, *Geophys. Res. Lett.*, 11 (5), 393-396, <https://doi.org/10.1029/GL011i005p00393>, 1984.

575 Satheesh, S., Moorthy, K. K.: Radiative effects of natural aerosols: A review, *Atmos. Environ.*, 39 (11), 2089-2110,  
576 <https://doi.org/10.1016/j.atmosenv.2004.12.029>, 2005.

577 Sharma, S., Ishizawa, M., Chan, D., Lavoué, D., Andrews, E., Eleftheriadis, K., and Maksyutov, S.: 16-year simulation of  
578 Arctic black carbon: Transport, source contribution, and sensitivity analysis on deposition, *J. Geophys. Res. Atmos.*, 118  
579 (2), 943-964, <https://doi.org/10.1029/2012JD017774>, 2013.

580 Shaw, G. E.: The Arctic haze phenomenon, *Bull. Amer. Meteorol. Soc.*, 76 (12), 2403-2414, [https://doi.org/10.1175/1520-0477\(1995\)076<2403:TAHP>2.0.CO;2](https://doi.org/10.1175/1520-0477(1995)076<2403:TAHP>2.0.CO;2), 1995.

582 Shen, L., Wang, H., Lu, S., Li, L., Yuan, J., Zhang, X., Tian, X., and Tang, Q.: Observation of aerosol size distribution and  
583 new particle formation at a coastal city in the Yangtze River Delta, China, *Sci. Total Environ.*, 565, 1175-1184,  
584 <https://doi.org/10.1016/j.scitotenv.2016.05.164>, 2016.

585 Shen, X., Sun, J., Zhang, X., Zhang, Y., Zhang, L., and Fan, R.: Key features of new particle formation events at background  
586 sites in China and their influence on cloud condensation nuclei, *Front. Environ. Sci Eng.*, 10 (5),  
587 <https://doi.org/10.1007/s11783-016-0833-2>, 2016.

588 Stanier, C. O., Khlystov, A. Y., and Pandis, S. N.: Nucleation Events During the Pittsburgh Air Quality Study: Description  
589 and Relation to Key Meteorological, Gas Phase, and Aerosol Parameters, *Aerosol Sci. Technol.*, 38 (sup1), 253-264,  
590 <https://doi.org/10.1080/02786820390229570>, 2004.

591 Stefels, J., Steinke, M., Turner, S., Malin, G., and Belviso, S.: Environmental constraints on the production and removal of the  
592 climatically active gas dimethylsulphide (DMS) and implications for ecosystem modelling, *Biogeochemistry*, 83 (1),  
593 245–275, <https://doi.org/10.1007/s10533-007-9091-5>, 2007.

594 Ström, J., Umegård, J., Tørseth, K., Tunved, P., Hansson, H. C., Holmén, K., Wisman, V., Herber, A., and König-Langlo,  
595 G.: One year of particle size distribution and aerosol chemical composition measurements at the Zeppelin Station,  
596 Svalbard, March 2000–March 2001, *Phys. Chem. Earth, Parts A/B/C* 2003, 28 (28-32), 1181-1190,  
597 <https://doi.org/10.1016/j.pce.2003.08.058>, 2003.

598 Ström, J., Engvall, A.-C., Delbart, F., Krejci, R., and Treffeisen, R.: On small particles in the Arctic summer boundary layer:  
599 observations at two different heights near Ny-Ålesund, Svalbard, *Tellus Ser. B-Chem. Phys. Meteorol.*, 61 (2), 473-482,  
600 <https://doi.org/10.3402/tellusb.v61i2.16845>, 2009.

601 IPCC, 2014: Climate Change 2014: Synthesis Report. Contribution of Working Groups I, II and III to the Fifth Assessment  
602 Report of the Intergovernmental Panel on Climate Change [Core Writing Team, R.K. Pachauri and L.A. Meyer (eds.)].  
603 IPCC, Geneva, Switzerland, 151 pp.

604 Toon, O. B. and Pollack, J. B.: Atmospheric aerosols and climate: Small particles in the Earth's atmosphere interact with visible  
605 and infrared light, altering the radiation balance and the climate, *American Scientist*, 68 (3), 268-278,  
606 <https://www.jstor.org/stable/27849822>, 1980.

607 Tovar-Sánchez, A., Duarte, C. M., Alonso, J. C., Lacorte, S., Tauler, R., and Galbán-Malagón, C.: Impacts of metals and  
608 nutrients released from melting multiyear Arctic sea ice, *J. Geophys. Res.*, 115 (C7),  
609 <https://doi.org/10.1029/2009JC005685>, 2010.

610 Tunved, P., Ström, J., and Krejci, R.: Arctic aerosol life cycle: linking aerosol size distributions observed between 2000 and  
611 2010 with air mass transport and precipitation at Zeppelin station, Ny-Ålesund, Svalbard, *Atmos. Chem. Phys.*, 13 (7),  
612 3643-3660, <https://doi.org/10.5194/acp-13-3643-2013>, 2013.

613 Uhlig, C., Damm, E., Peeken, I., Krumpfen, T., Rabe, B., Korhenon, M., and Ludwighowski, K.-U.: Sea Ice and Water Mass  
614 Influence Dimethylsulphide Concentration in the Central Arctic Ocean, *Front. Earth Sci.*, 7, 179,  
615 <https://doi.org/10.3389/feart.2019.00179>, 2019.

616 Vehkamäki, H., Dal Maso, M., Hussein, T., Flanagan, R., Hyvärinen, A., Lauros, J., Merikanto, P., Mönkkönen, M., Pihlatie,  
617 K., Salminen, K., Sogacheva, L., Thum, T., Ruuskanen, T. M., Keronen, P., Aalto, P. P., Hari, P., Lehtinen, K. E. J.,  
618 Rannik, Ü., and Kulmala, M.: Atmospheric particle formation events at Värriö measurement station in Finnish Lapland  
619 1998–2002, *Atmos. Chem. Phys.*, 4, 2015–2023, <https://doi.org/10.5194/acp-4-2015-2004>, 2004.

620 Venzac, H., Sellegri, K., Laj, P., Villani, P., Bonasoni, P., Marinoni, A., Cristofanelli, P., Calzolari, F., Fuzzi, S., and Decesari,  
621 S.: High frequency new particle formation in the Himalayas, *Proc. Natl. Acad. Sci.*, 105 (41), 15666-15671,  
622 <https://doi.org/10.1073/pnas.0801355105>, 2008.

623 Wang, Y., Zhang, X., and Draxler, R. R.: TrajStat: GIS-based software that uses various trajectory statistical analysis methods  
624 to identify potential sources from long-term air pollution measurement data, *Environ. Modelling Softw.*, 24 (8), 938-939,  
625 <https://doi.org/10.1016/j.envsoft.2009.01.004>, 2009.

626 Wang, Z., Wu, Z., Yue, D., Shang, D., Guo, S., Sun, J., Ding, A., Wang, L., Jiang, J., Guo, H., Gao, J., Cheung, H. C.,  
627 Morawska, L., Keywood, M., and Hu, M.: New particle formation in China: Current knowledge and further directions,  
628 *Sci. Total Environ.*, 577, 258-266, <https://doi.org/10.1016/j.scitotenv.2016.10.177>, 2017.

629 Weller, R., Schmidt, K., Teinilä, K., and Hillamo, R.: Natural new particle formation at the coastal Antarctic site Neumayer,  
630 *Atmos. Chem. Phys.*, 15 (19), 11399-11410, <https://doi.org/10.5194/acp-15-11399-2015>, 2015.

631 Wiedensohler, A., Covert, D. S., Swietlicki, E., Aalto, P., Heintzenberg, J., and Leck, C.: Occurrence of an ultrafine particle  
632 mode less than 20 nm in diameter in the marine boundary layer during Arctic summer and autumn, *Tellus Ser. B-Chem.*  
633 *Phys. Meteorol.*, 48 (2), 213-222, <https://doi.org/10.3402/tellusb.v48i2.15887>, 1996.

634 Willis, M. D., Burkart, J., Thomas, J. L., Köllner, F., Schneider, J., Bozem, H., Hoor, P. M., Aliabadi, A. A., Schulz, H., and  
635 Herber, A. B.: Growth of nucleation mode particles in the summertime Arctic: a case study, *Atmos. Chem. Phys.*, 16 (12),  
636 7663-7679, <https://doi.org/10.5194/acp-16-7663-2016>, 2016.

637 Woo, K. S., Chen, D. R., Pui, D. Y. H., and McMurry, P. H.: Measurement of Atlanta Aerosol Size Distributions: Observations  
638 of Ultrafine Particle Events, *Aerosol Sci. Technol.*, 34 (1), 75-87, <https://doi.org/10.1080/02786820120056>, 2010.

639 Wu, Z., Hu, M., Liu, S., Wehner, B., Bauer, S., Maßling, A., Wiedensohler, A., Petäjä, T., Dal Maso, M., and Kulmala, M.:  
640 New particle formation in Beijing, China: Statistical analysis of a 1-year data set, *J. Geophys. Res.: Atmos.*, 112 (D9),  
641 <https://doi.org/10.1029/2006JD007406>, 2007.

642 Xiao, S., Wang, M. Y., Yao, L., Kulmala, M., Zhou, B., Yang, X., Chen, J. M., Wang, D. F., Fu, Q. Y., Worsnop, D. R., and  
643 Wang, L.: Strong atmospheric new particle formation in winter in urban Shanghai, China, *Atmos. Chem. Phys.*, 15 (4),  
644 1769-1781, <https://doi.org/10.5194/acp-15-1769-2015>, 2015.

645 Yu, H., Ren, L., and Kanawade, V. P.: New particle formation and growth mechanisms in highly polluted environments, *Curr.*  
646 *Pollut. Rep.*, 3 (4), 245-253, <https://doi.org/10.1007/s40726-017-0067-3>, 2017.

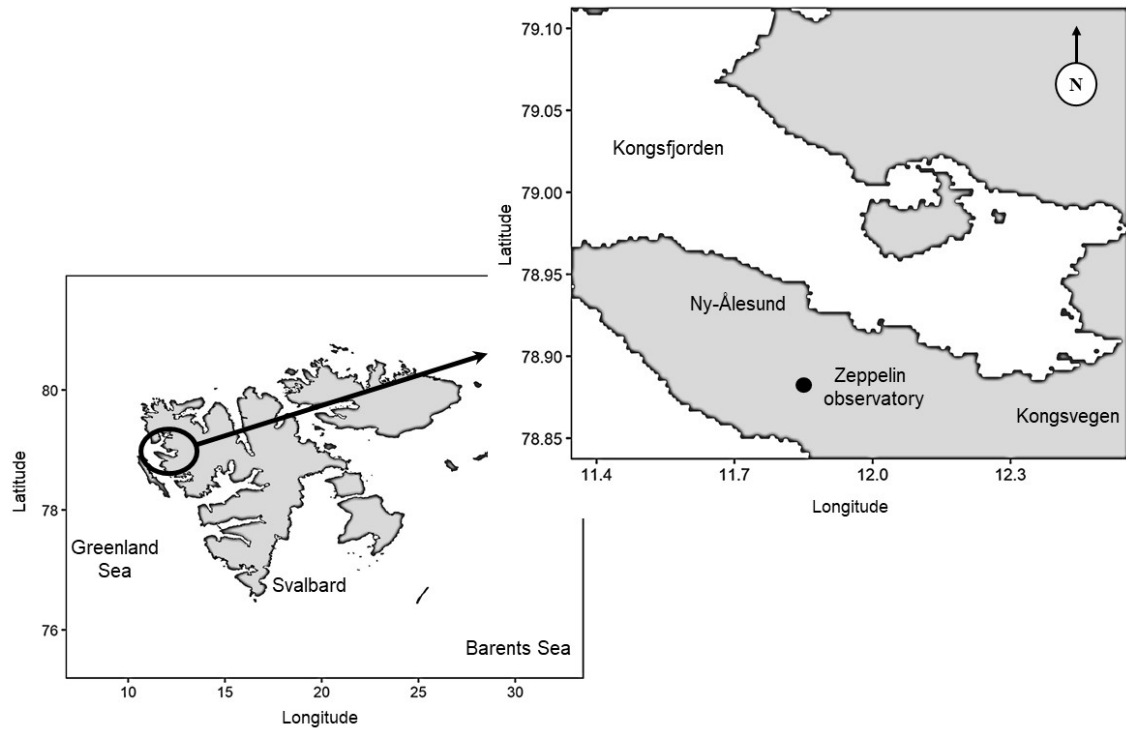
647 Zhan, J., Li, W., Chen, L., Lin, Q., and Gao, Y.: Anthropogenic influences on aerosols at Ny-Ålesund in the summer Arctic,  
648 *Atmos. Pollut. Res.*, 8, 383-393, <http://dx.doi.org/10.1016/j.apr.2016.10.010>, 2017.

649 Zhang, Y., Zhang H.-H., Yang G.-P., and Liu Q.-L.: Chemical Characteristics and Source Analysis of Aerosol Composition  
650 over the Bohai Sea and the Yellow Sea in Spring and Autumn, *J. Atmos. Sci.*, 72 (9), 3563-3573,  
651 <https://doi.org/10.1175/JAS-D-14-0372.1>, 2015.

652 Zhang, M., Park, K.-T., Lin, Q., Yan, J., Park, K., Wu, Y., Chen, L., Jang, E., Gao, W., Tan, G., and Wang, J.: Atmospheric  
653 dimethyl sulfide and its significant influence on the sea-to-air flux calculation over the Southern Ocean. *Prog. Oceanogr.*,  
654 186, <https://doi.org/10.1016/j.pocean.2020.102392>, 2020.

655



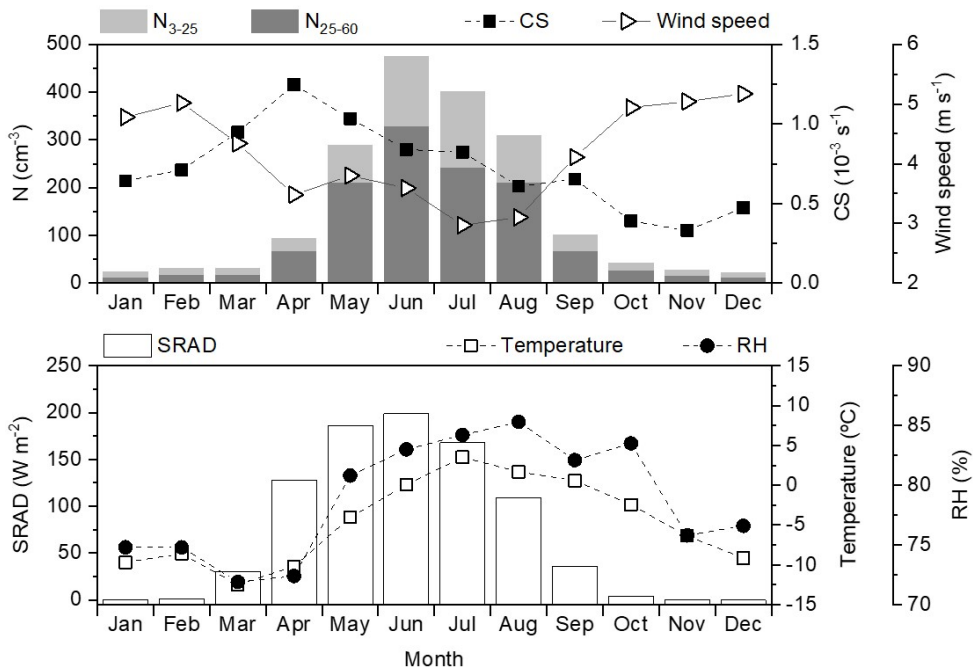


656

657 Figure 1. Measurement site (Zeppelin Observatory) in the Svalbard Archipelago, Ny-Ålesund, Norway.

658

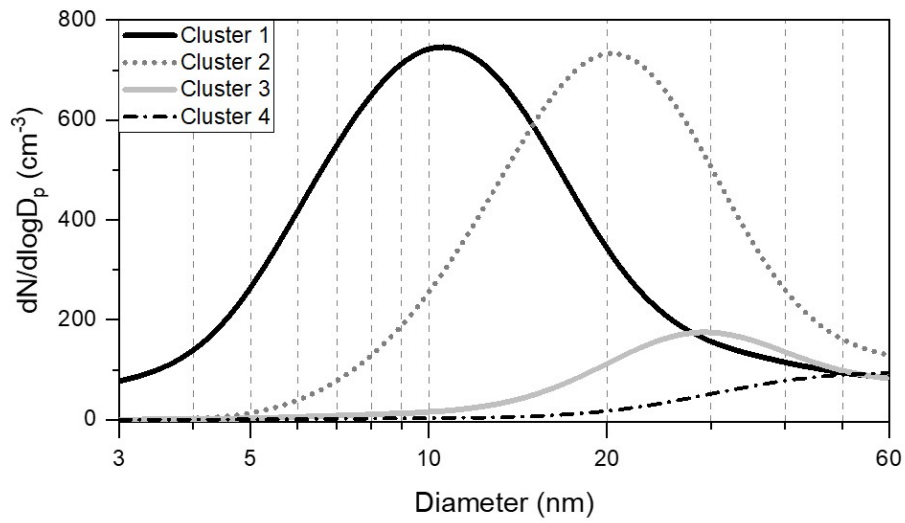




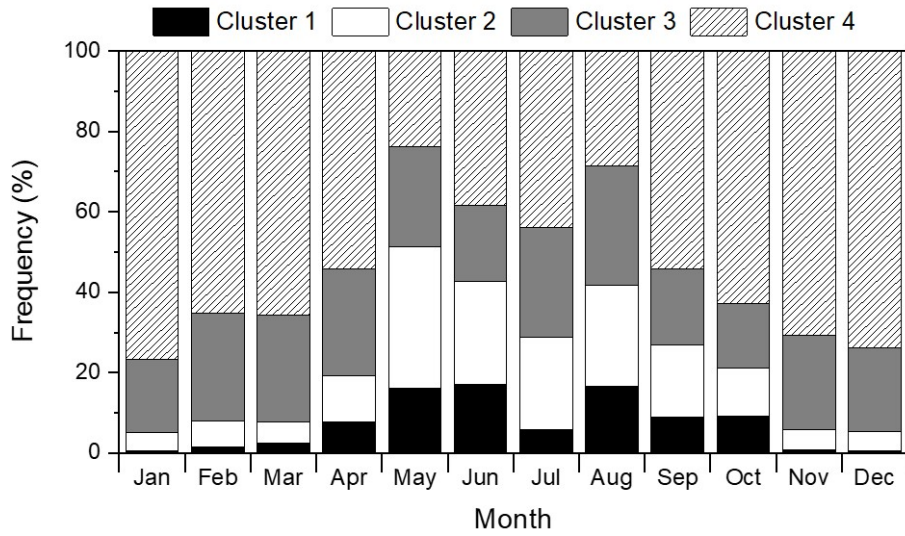
659

660 Figure 2. Monthly variations of  $N_{3-25}$ ,  $N_{25-60}$ , CS, and wind speed (upper panel), temperature, RH, and SRAD (lower panel)  
 661 from 2016 to 2018.

662



(a)

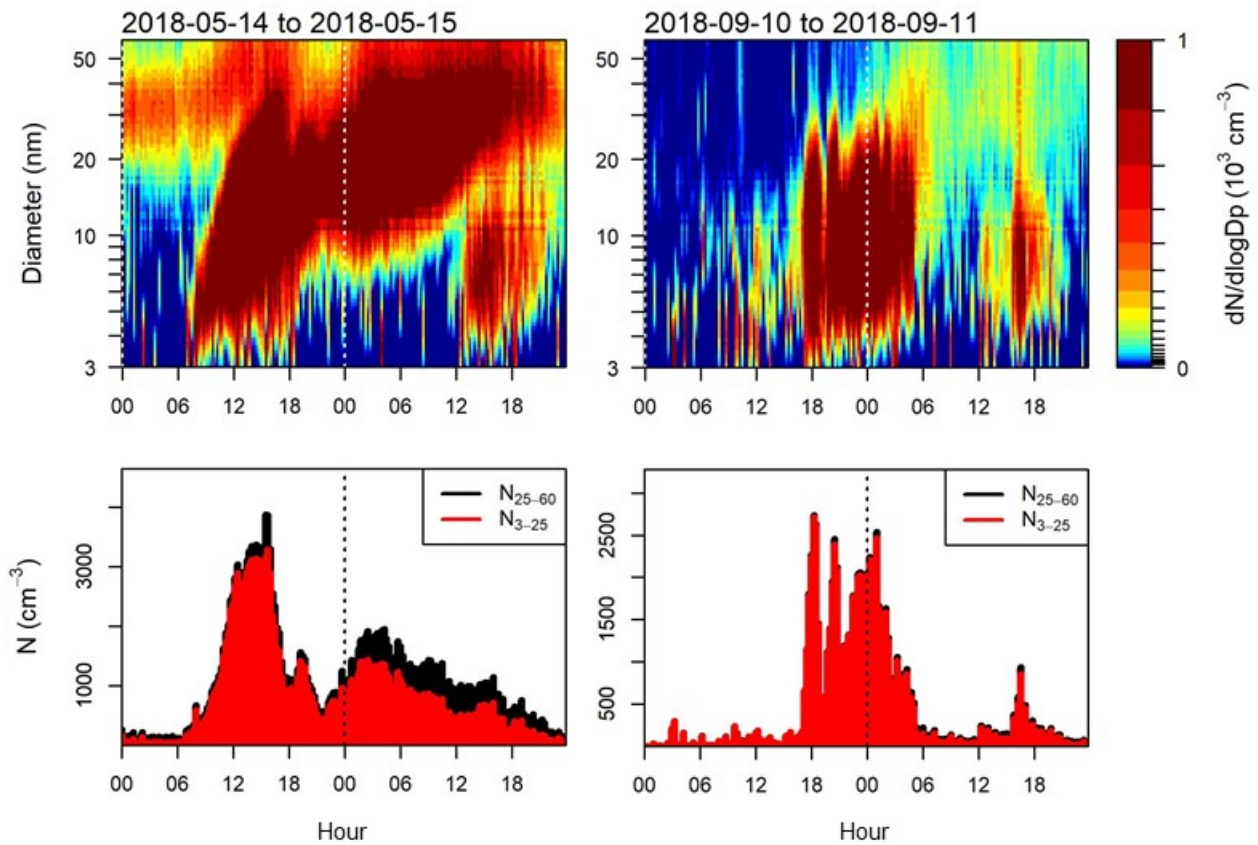


(b)

663  
664

665  
666  
667  
668

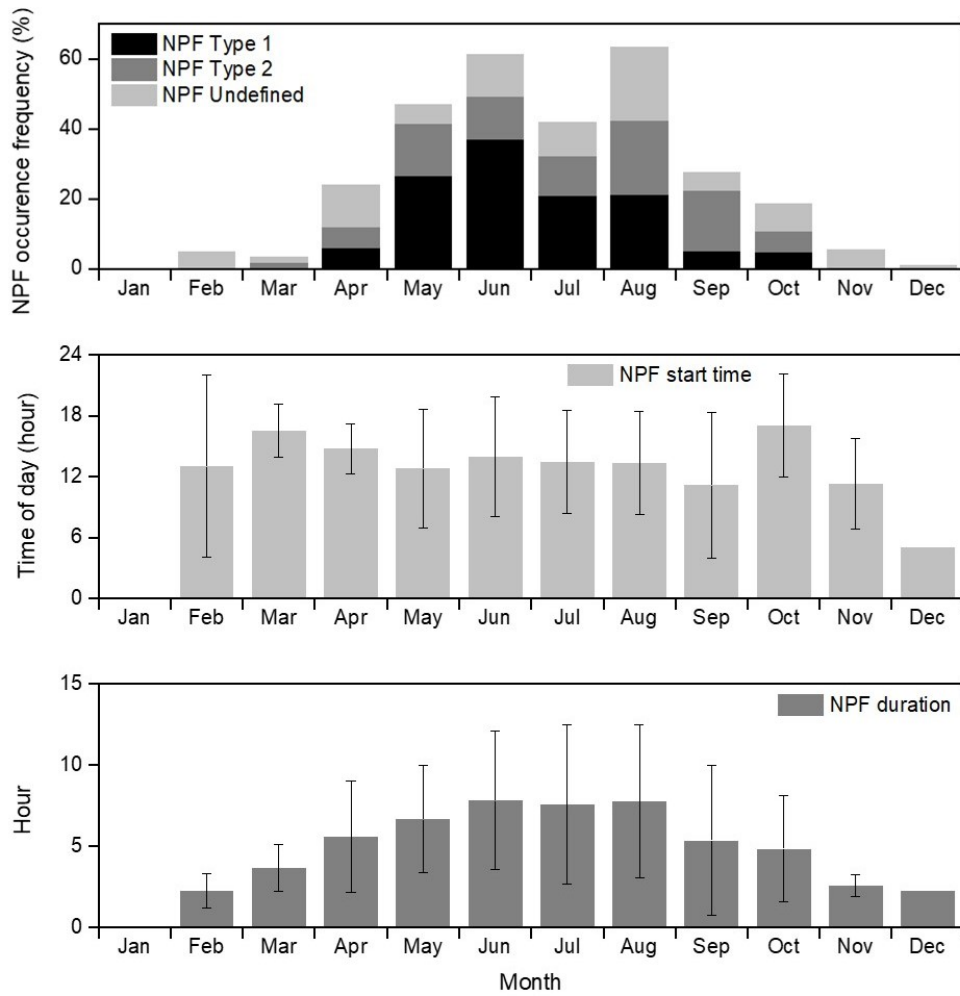
Figure 3. Major particle clusters by (a) size distribution and (b) monthly frequency of clusters from 2016 to 2018.



669

670 Figure 4. Examples of distinct NPF types identified in this study. In type 1 (left),  $N_{3-25}$  increases significantly with continuous  
 671 particle growth, while in type 2 (right) it increases significantly without significant particle growth. The x-axis is the local time  
 672 (hour).

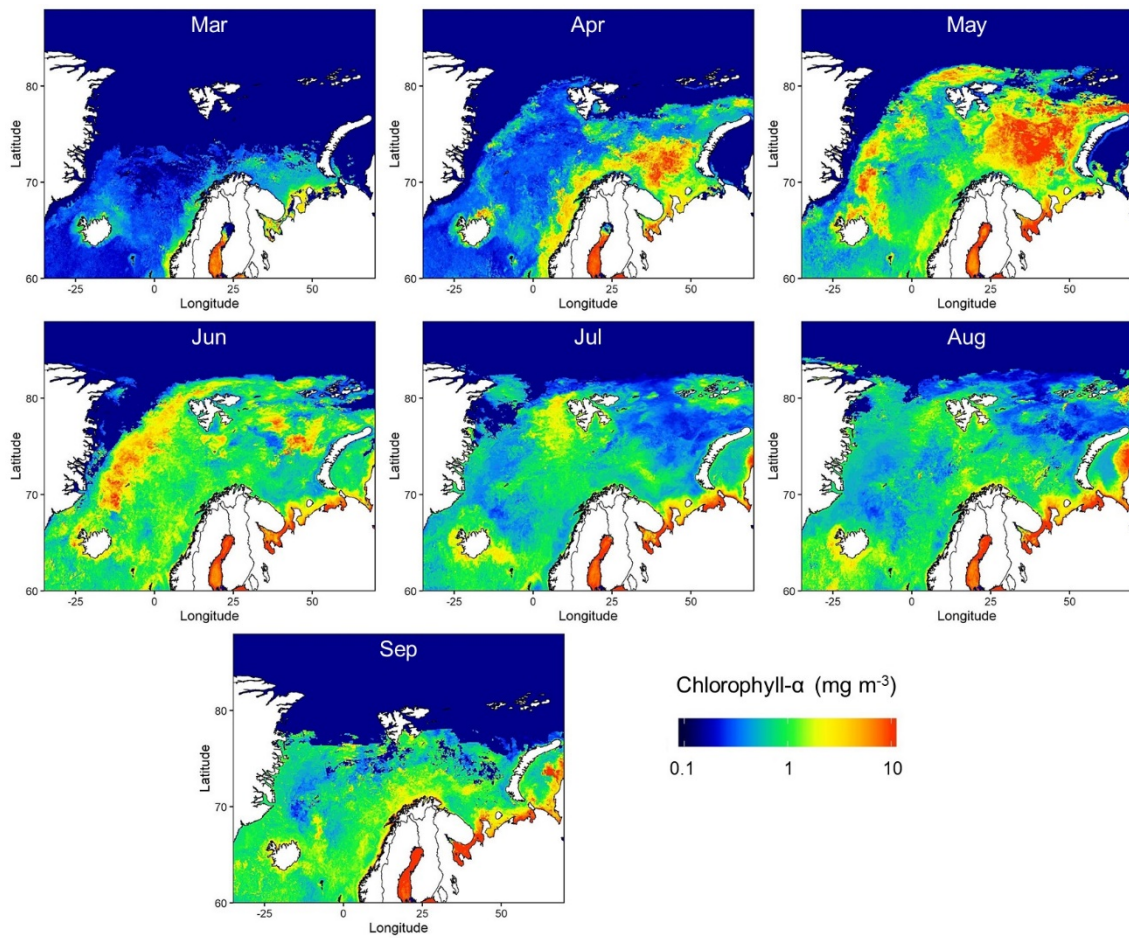
673



674

675 Figure 5. Monthly variations of NPF occurrence, start time (local time), and duration; the error bar represents standard  
 676 deviation.

677



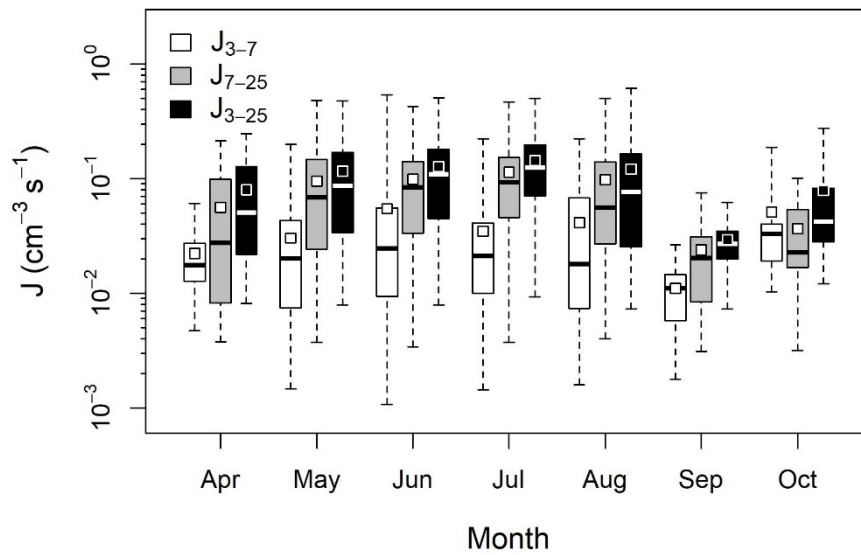
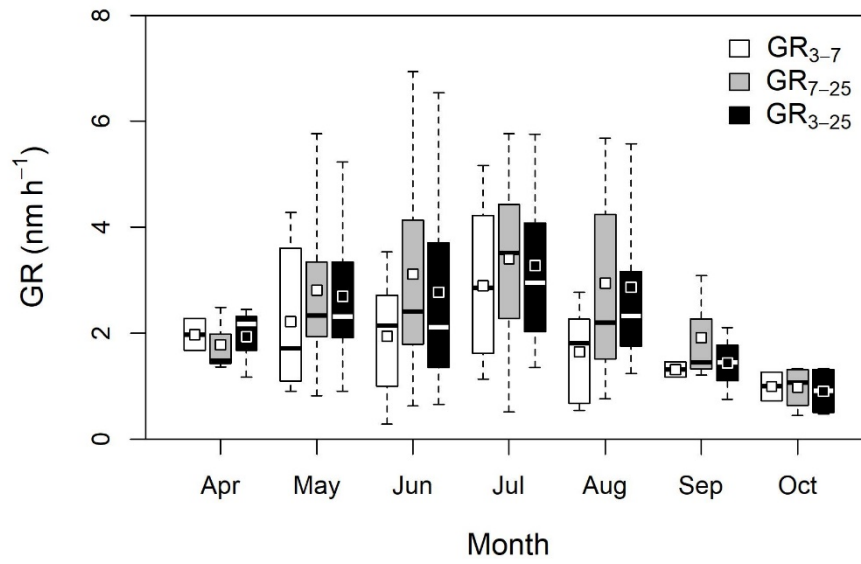
678

679 Figure 6. MODIS-derived monthly chlorophyll- $\alpha$  concentration from 2016 to 2018 at 4 km resolution.

680

681

682



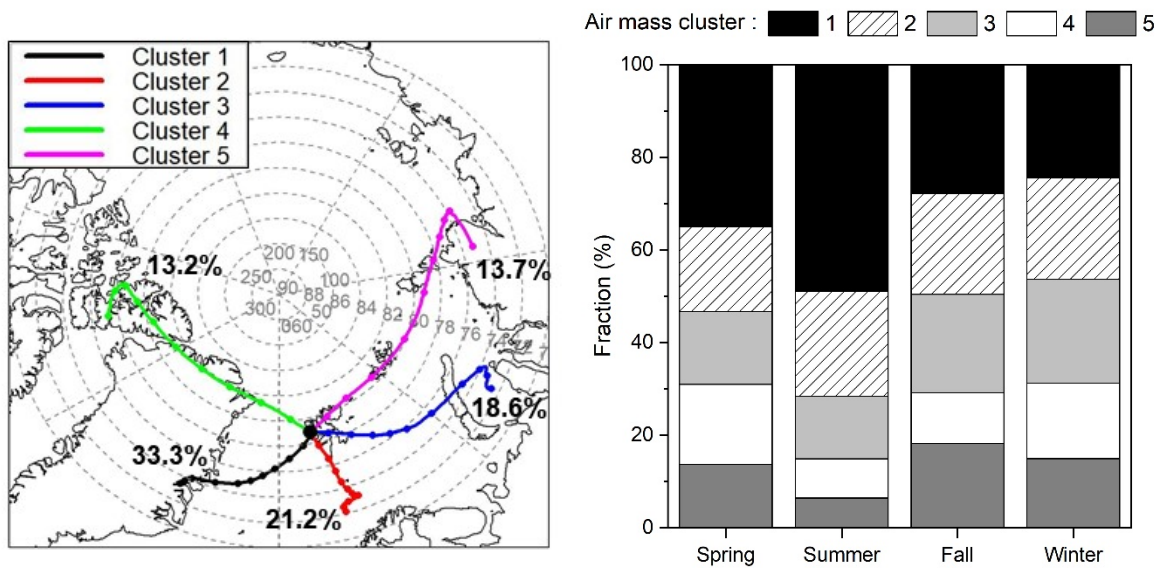
683

684

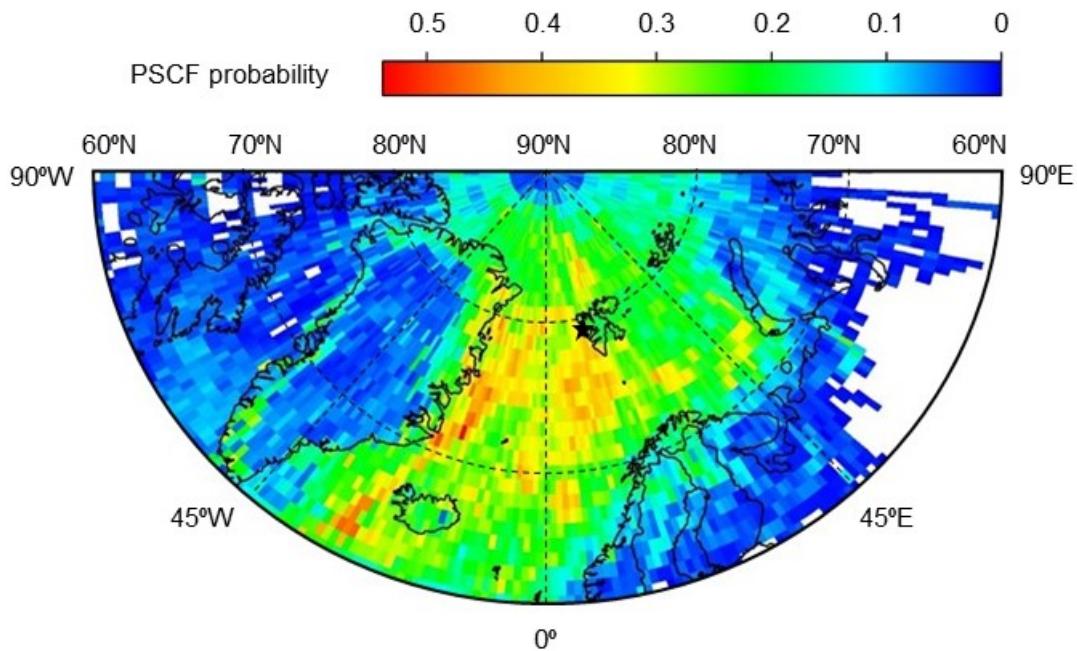
685 Figure 7. Monthly variations of  $GR_{3-7}$ ,  $GR_{7-25}$ ,  $GR_{3-25}$ ,  $J_{3-7}$ ,  $J_{7-25}$ , and  $J_{3-25}$  for NPF in the Arctic. Boxes and whiskers represent  
 686 the 25<sup>th</sup>–75<sup>th</sup> percentiles and minimum–maximum, respectively; squares indicate means and horizontal lines within boxes  
 687 indicate medians.

688





(a)



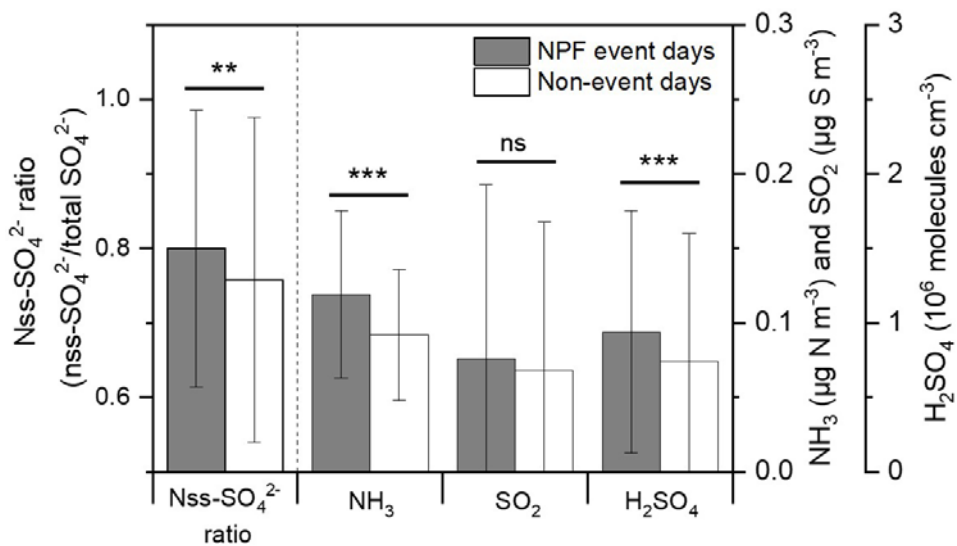
(b)

689  
690

691  
692  
693  
694  
695

Figure 8. (a) Five major clusters for air mass back trajectories from 2016 to 2018 and the fraction of each cluster by seasons. (b) PSCF back-trajectory analysis for air mass origins affecting NPF at the 75<sup>th</sup> percentile of  $N_{3-25}$ .

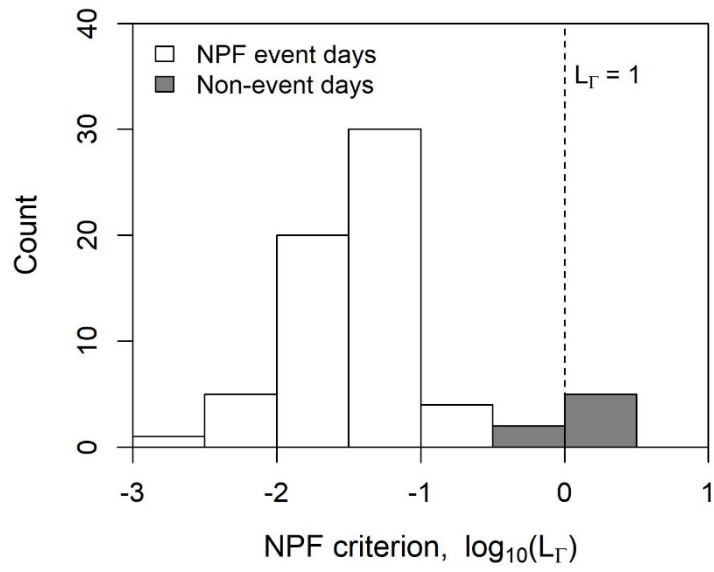




696

697 Figure 9. Comparison of average nss-SO<sub>4</sub><sup>2-</sup> ratio (nss-SO<sub>4</sub><sup>2-</sup>/total SO<sub>4</sub><sup>2-</sup>), NH<sub>3</sub>, SO<sub>2</sub>, and H<sub>2</sub>SO<sub>4</sub> concentrations between NPF  
 698 events and non-event days: error bar and stars represent the standard deviation and *p*-values of a t-test (ns: > 0.05, \*: ≤ 0.05,  
 699 \*\*: ≤ 0.01, \*\*\*: ≤ 0.001), respectively.

700



701

702 Figure 10. Distribution of NPF criterion ( $L_\Gamma$ ) values for NPF event days (white) and non-event days (grey) in the Arctic.

703

Table 1. Summary of NPF frequency, J, and GR at various sampling sites, including the present study.

Site name and characteristics		Period	NPF frequency	GR (nm h <sup>-1</sup> )		J (cm <sup>-3</sup> s <sup>-1</sup> )		Reference
Zeppelin, Norway	Arctic	2016 to 2018	23%	GR <sub>3-7</sub>	0.29–5.17	J <sub>3-7</sub>	0.001–0.54	This study
				GR <sub>7-25</sub>	0.45–6.94	J <sub>7-25</sub>	0.003–0.50	
				GR <sub>3-25</sub>	0.48–6.54	J <sub>3-25</sub>	0.007–0.61	
Finokalia, Greece	Marine background	Jun 2008 to Jun 2018	27%	GR <sub>9-25</sub>	5.4±3.9	J <sub>9-25</sub>	0.9±1.2	Kalivitis et al. (2019)
Beijing, China	Urban	Mar 2004 to Feb 2005	40%	GR <sub>3-25</sub>	0.1–11.2	J <sub>3-25</sub>	3.3–81.4	Wu et al. (2007)
Pittsburgh, USA	Urban	Jul 2001 to Jun 2002	30%	N/A	N/A	N/A	N/A	Stanier et al. (2004)
San Pietro Capofiume, Italy	Sub-urban	Mar 2002 to Mar 2005	36%	GR <sub>3-20</sub>	2.9–22.9	J <sub>3-20</sub>	0.2–36.9	Hamed et al. (2007)
12 European sites (EUCAARI project) <sup>a</sup>	Rural and background	2008 to 2009	21–57%	GR <sub>7-20</sub>	3.6–6.8	J <sub>2-3</sub>	0.7–32.4	Manninen et al. (2010)
Hyytiälä, Finland	Rural	1996 to 2003	>24%	GR <sub>3-25</sub>	0.9–5.3	J <sub>3-25</sub>	0.2–1.1	Dal Maso et al. (2005)
ShangDianzi station, China	Rural	Mar 2008 to Dec 2013	36%	GR <sub>3-25</sub>	0.7–13.4	J <sub>3-25</sub>	0.5–39.3	Shen et al. (2016)
Pyramid, Nepal	Himalayas	Mar 2006 to Aug 2007	>35%	GR <sub>10-20</sub>	1.8 ± 0.7	J <sub>10-20</sub>	0.05–0.2	Venzac et al. (2008)
Dome C	Antarctica	Dec 2007 to Nov 2009	5–54%	GR <sub>10-25</sub>	0.5–4.6	J <sub>10-25</sub>	0.022–0.11	Järvinen et al. (2013)

Neumayer	Antarctic <sup>a</sup>	Jan 2012 to Mar 2012 Feb 2014 to Apr 2014	N/A	GR <sub>3-25</sub>	0.4–1.9	J <sub>3-25</sub>	0.02–0.1	Weller et al. (2015)
King Sejong	Antarctic <sup>a</sup>	Mar 2009 to Dec 2016	6%	GR <sub>10-25</sub>	0.02–3.09	J <sub>2.5-10</sub>	0.16-9.88	Kim et al. (2019)
Nord, Greenland	Arctic	Jul 2010 to Feb 2013	17–38%	N/A	N/A	N/A	N/A	Nguyen et al. (2016)

705 <sup>a</sup> Pallas and Hyttiälä (Finland), Vavilhill (Sweden), Mace Head (Ireland), Cavauw (Netherlands), Melpitz and Hohenpeissenberg (Germany), K-Pusztá (Hungary), Jungfraujoch (Switzerland), Puy de Dome (France), San Pietro Capofiume (Italy), and Finokalia (Greece).

*Supplement of*  
**Atmospheric new particle formation characteristics in the Arctic as  
measured at Mount Zeppelin, Svalbard, from 2016 to 2018**

Haebum Lee et al.

*Correspondence to:* Kihong Park (kpark@gist.ac.kr) and Young-Jun Yoon (yjyoon@kopri.re.kr)

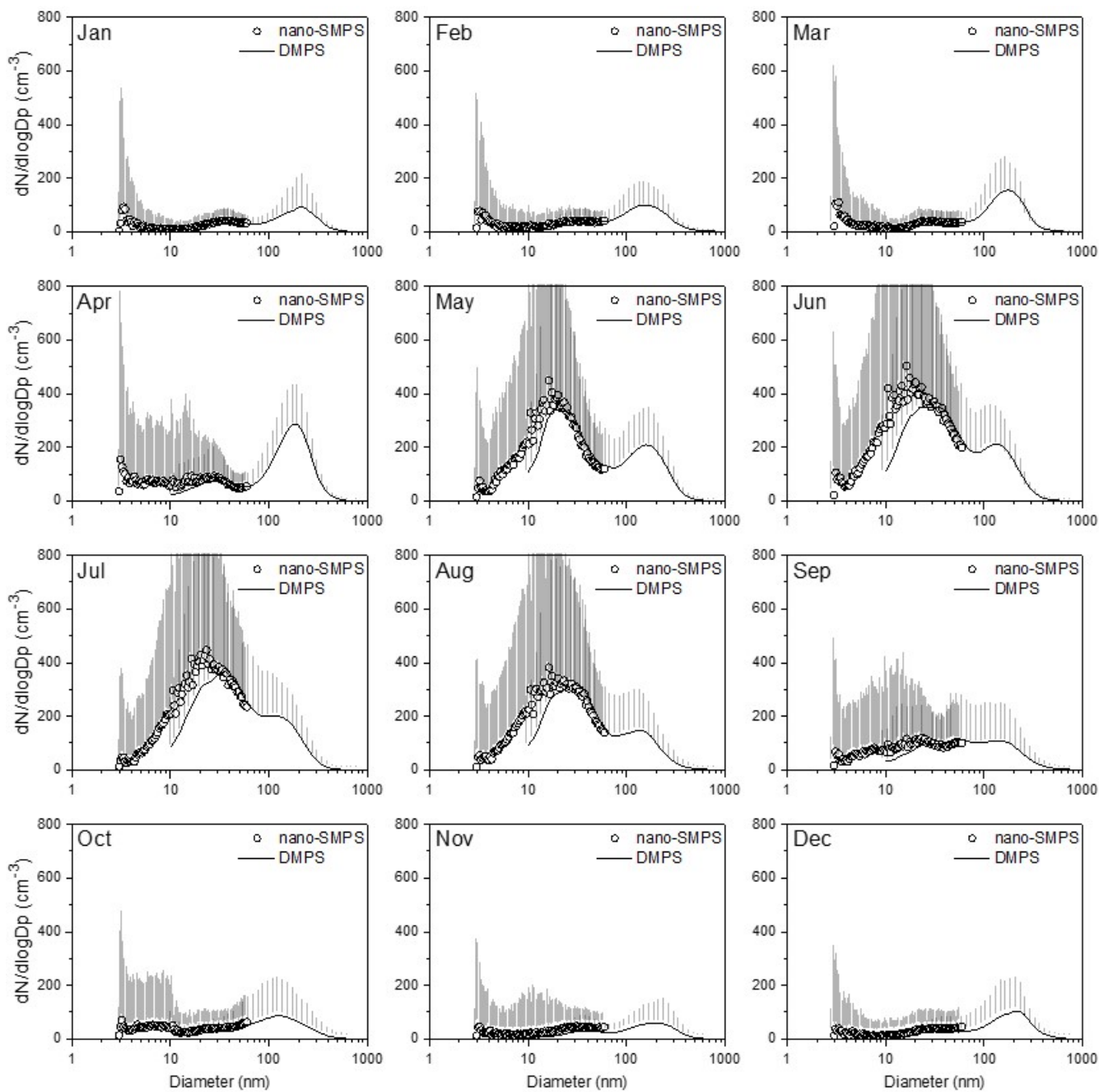


Figure S1. Comparison of monthly average size distributions obtained from the nano-SMPS (3–60 nm) and DMPS (10–810 nm). The error bar indicates standard deviation.

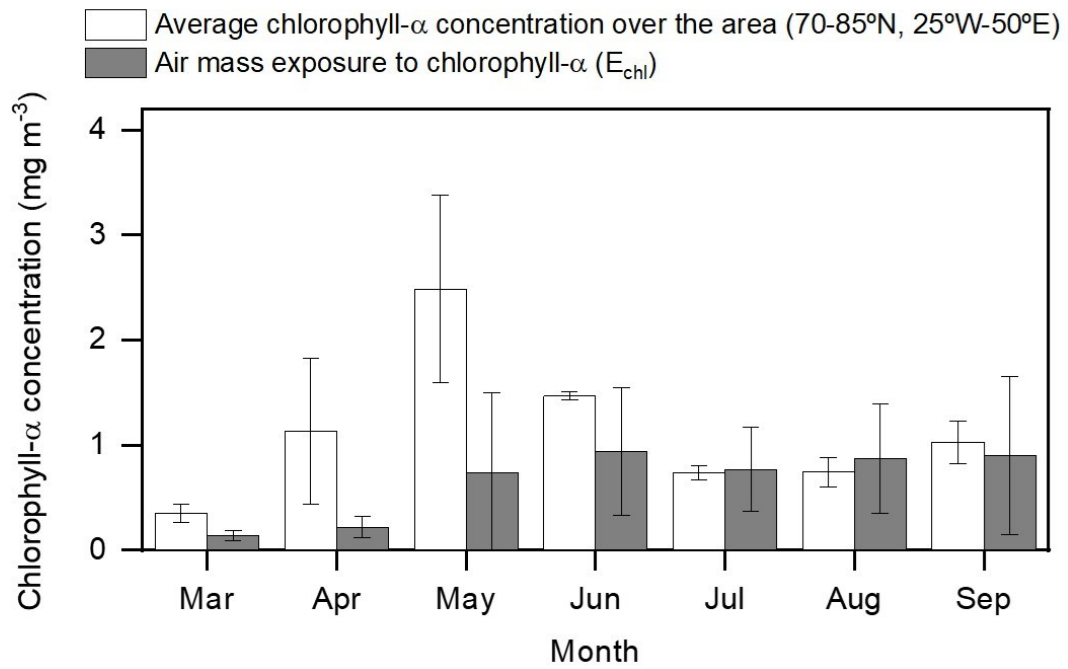


Figure S2. Monthly values of average chlorophyll- $\alpha$  concentration over the area (70-85°N, 25°W-50°E) and “air mass exposure to chlorophyll- $\alpha$ ” ( $E_{chl}$ ) calculated by Eq. (1) in Park et al. (2018) from March to September 2016 to 2018.



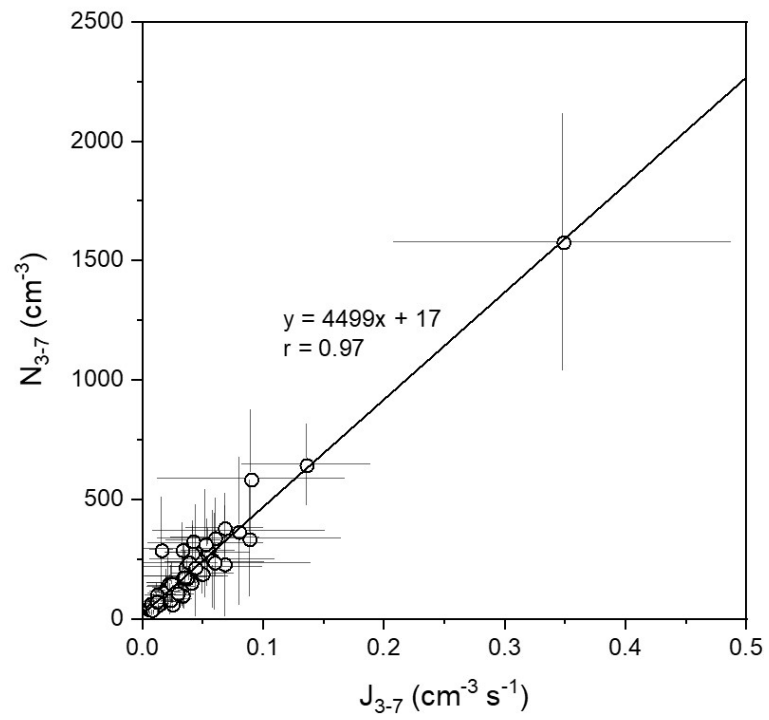
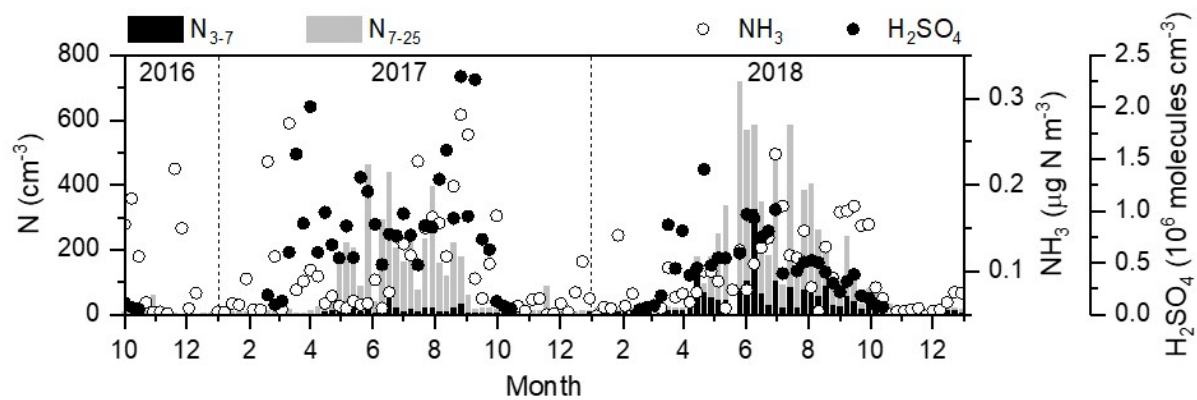
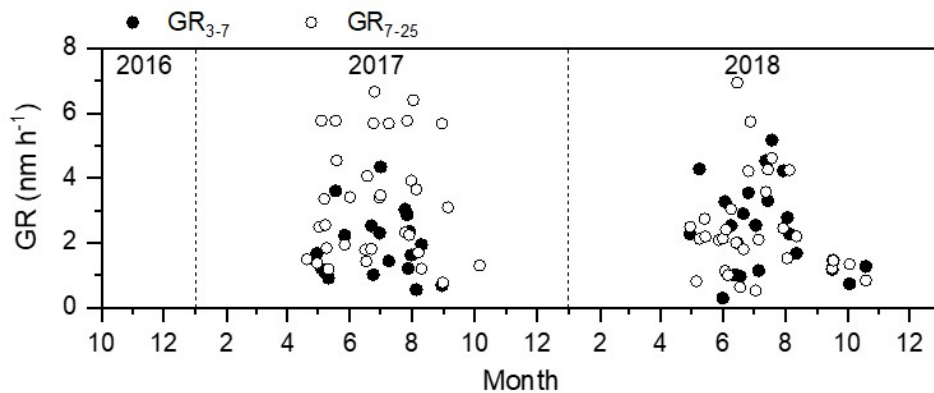


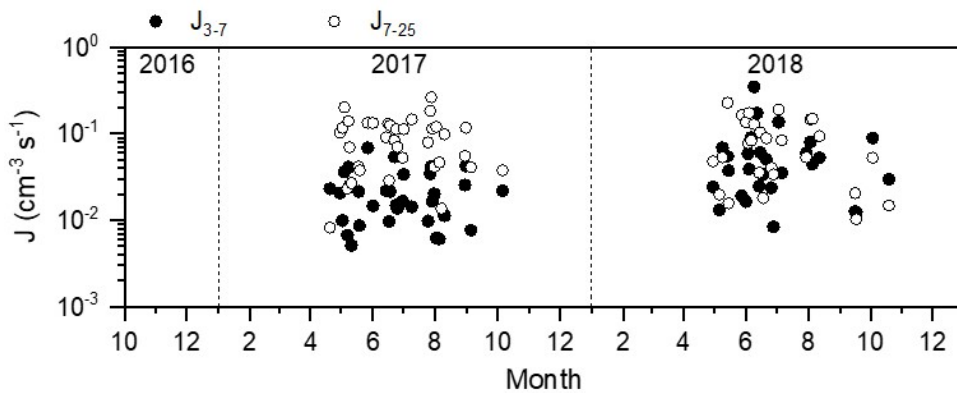
Figure S3. Relationship between  $N_{3-7}$  and  $J_{3-7}$  during NPF events with a linear regression line and a correlation coefficient ( $r$ ).



(a)

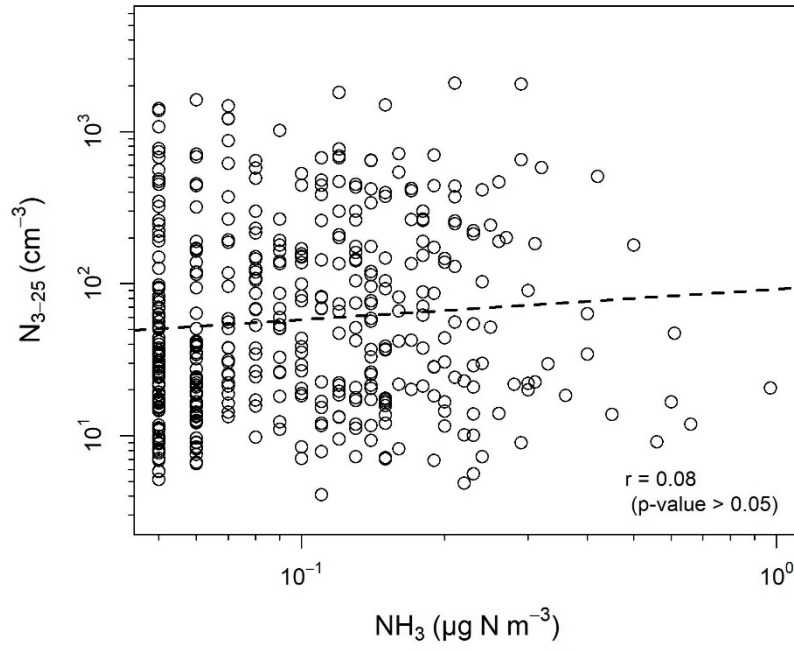


(b)

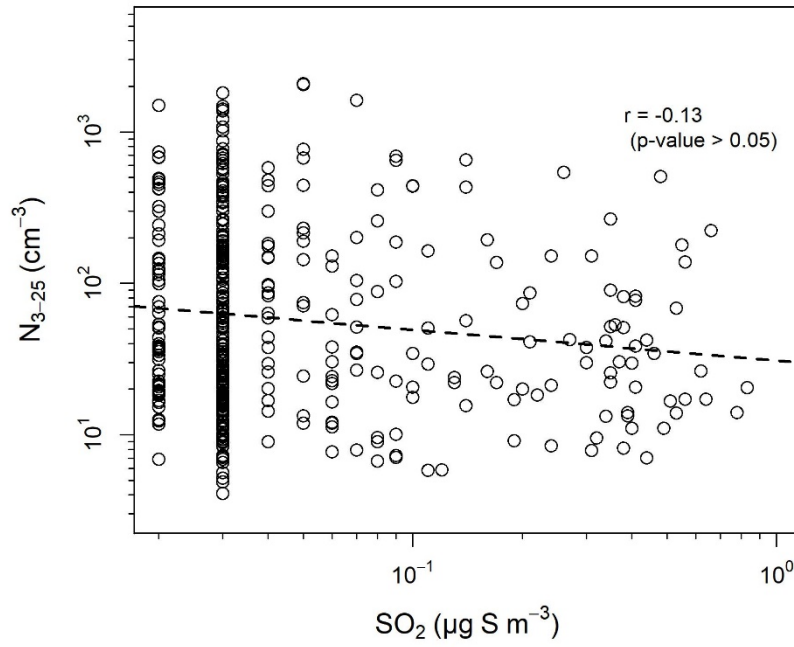


(c)

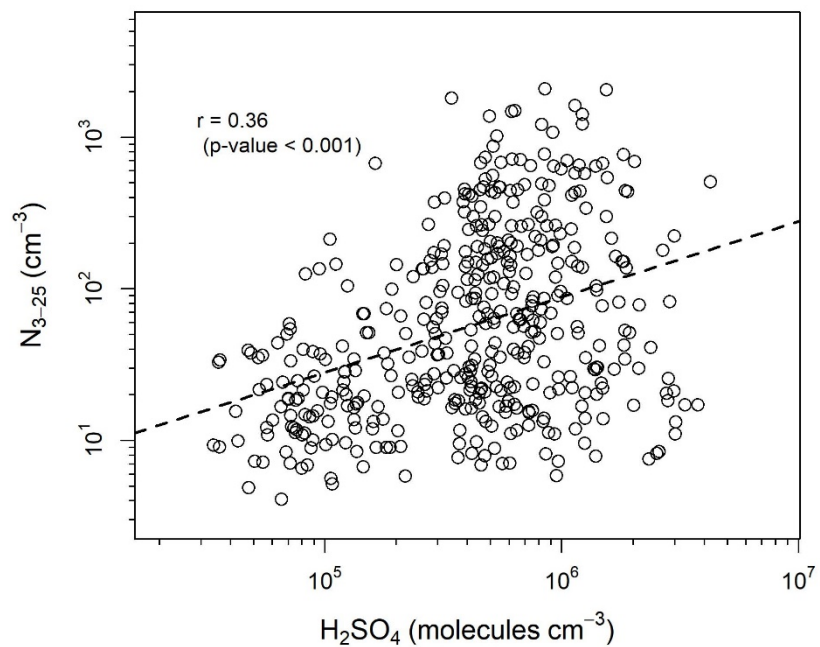
Figure S4. Time series of (a) weekly  $N_{3-7}$ ,  $N_{7-25}$ ,  $NH_3$ , and  $H_2SO_4$ , (b) daily GR and (c) daily J in different modes ( $J_{3-7}$ ,  $J_{7-25}$ ,  $GR_{3-7}$ , and  $GR_{7-25}$ ).



(a)



(b)



(c)

Figure S5. Correlations of daily  $N_{3-25}$  versus (a) daily  $NH_3$ , (b) daily  $SO_2$ , and (c) daily  $H_2SO_4$  concentrations during the measurement period. The dashed line represents a linear regression line with a correlation coefficient ( $r$ ).

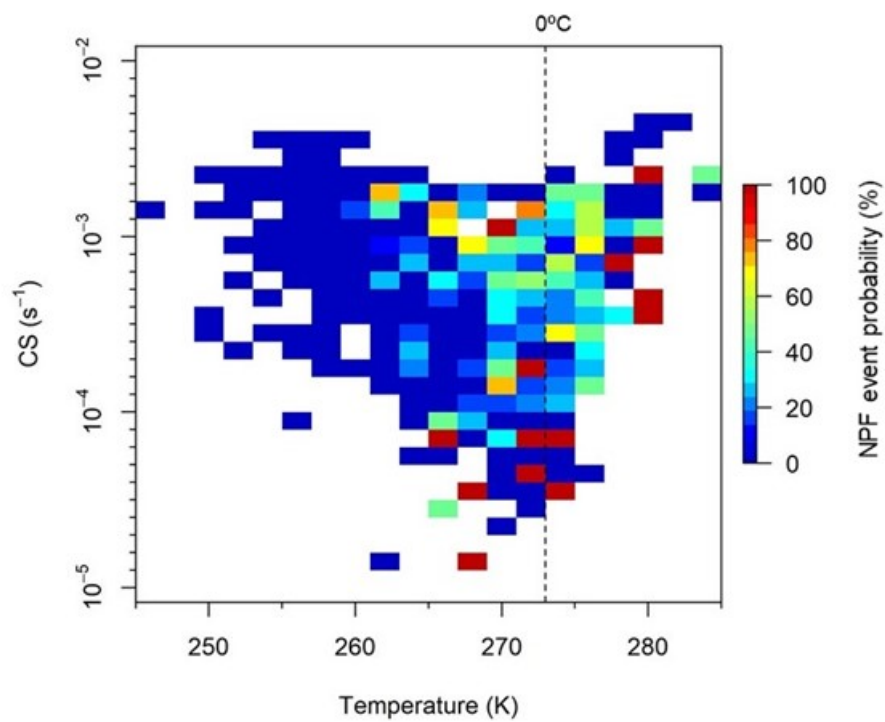


Figure S6. NPF event probability distribution with daily CS and temperature. The cell size was 2 K (temperature) and the ratio of 1.26 between two consecutive CS values.

Table S1. Average concentrations of ionic species ( $\text{Na}^+$ ,  $\text{Mg}^{2+}$ ,  $\text{K}^+$ ,  $\text{NH}_4^+$ ,  $\text{NO}_3^-$ ,  $\text{SO}_4^{2-}$ , and  $\text{Cl}^-$ ) in particulate matter and gaseous species ( $\text{NH}_3$ ,  $\text{SO}_2$ , and  $\text{H}_2\text{SO}_4$ ) in different seasons from 2016 to 2018.

	Unit	Spring	Summer	Fall	Winter
$\text{Na}^+$	$\mu\text{g m}^{-3}$	0.27±0.38	0.18±0.28	0.22±0.28	0.31±0.33
$\text{Mg}^{2+}$	$\mu\text{g m}^{-3}$	0.04±0.08	0.02±0.04	0.03±0.04	0.05±0.05
$\text{K}^+$	$\mu\text{g m}^{-3}$	0.05±0.07	0.03±0.02	0.03±0.02	0.03±0.02
$\text{NH}_4^+$	$\mu\text{g N m}^{-3}$	0.04±0.05	0.02±0.03	0.02±0.03	0.02±0.02
$\text{NO}_3^-$	$\mu\text{g N m}^{-3}$	0.02±0.02	0.02±0.02	0.02±0.04	0.02±0.02
$\text{SO}_4^{2-}$	$\mu\text{g S m}^{-3}$	0.19±0.18	0.08±0.10	0.08±0.09	0.11±0.20
$\text{Cl}^-$	$\mu\text{g m}^{-3}$	0.39±0.63	0.24±0.43	0.35±0.50	0.52±0.59
$\text{NH}_3$	$\mu\text{g N m}^{-3}$	0.13±0.60	0.16±0.22	0.10±0.10	0.08±0.07
$\text{SO}_2$	$\mu\text{g S m}^{-3}$	0.09±0.22	0.08±0.11	0.08±0.13	0.09±0.27
$\text{H}_2\text{SO}_4$	$10^5 \text{ molecules cm}^{-3}$	7.43±8.16	8.59±8.64	5.52±8.91	0.95±0.69